

This report has been reproduced directly from the best available copy.

Available to DOE and DOE contractors from the Office Of Scientific and Technical Information, P.O. Box 62, Oak Ridge, TN 37831; prices available from (615)576-8401, FTS 626-8401.

Available to the public from the National Technical Information Service, U.S. Department of Commerce, 5285 Port Royal Rd., Springfield, VA 22161

Price: Printed A04
Microfiche A01

**A STUDY OF STEADY-STATE STEAM-WATER COUNTERFLOW
IN POROUS MEDIA**

Topical Report

**By
Cengiz Satik
Mehmet Parlar
Yanis C. Yortsos**

February 1990

Work Performed Under Contract No. FG19-87BC14126

**Prepared for
U.S. Department of Energy
Assistant Secretary for Fossil Energy**

**Thomas B. Reid, Project Manager
Bartlesville Project Office
P.O. Box 1398
Bartlesville, OK 74005**

**Prepared by
University of Southern California
Department of Petroleum Engineering
Los Angeles, CA 90089-1211**

TABLE OF CONTENTS

	PAGE
ABSTRACT.....	1
INTRODUCTION.....	2
FORMULATION.....	4
HEAT PIPE PROBLEM.....	9
GEOHERMAL PROBLEM.....	21
CONCLUSIONS.....	25
NOMENCLATURE.....	27
REFERENCES.....	29
APPENDIX.....	32
TABLE 1.....	33

FIGURES

Figure 1. Countercurrent Flow Schematic.....	34
Figure 2. Schematics of Capillary Pressure (a) and Relative Permeability Curves (b).....	35
Figure 3. Boundary Layer Profiles: Normalized Vapor Flux (a) and Evaporation Rate (b).....	36
Figure 4. Profiles Corresponding to Ref. [18]: Temperature (a) and Liquid Saturation (b). Dots in (a) Correspond to Experimental Points [18].....	37
Figure 5. Critical Heat Flux as a Function of Permeability for	

Bottom Heating.....	38
Figure 6. Effect of Surface Tension (a: $\sigma= 14.7275, 29.455, 58.91, 117.82$, from left to right) and Imposed Pressure (b: $P_o= 80, 50, 30, 15$, from left to right) on the Critical Heat Flux Curve.....	39
Figure 7. Critical Heat Flux as a Function of Permeability for Top Heating.....	40
Figure 8. Composite Schematic of Critical Heat Flux Curve for Both Top and Bottom Heating.....	41
Figure 9. Solution Trajectories for Bottom Heating and $\omega=0.1$: Temperature vs. Saturation (a) and Saturation vs. Distance (b). The Solid Curves in (a) Correspond to $G = 0$	42
Figure 10. Solution Trajectories for Bottom Heating and $\omega=0.4$: Temperature vs. Saturation (a) and Saturation vs. Distance (b). The Solid Curves in (a) Correspond to $G = 0$	43
Figure 11. Solution Trajectories for Bottom Heating and $\omega=0.5$: Temperature vs. Saturation (a) and Saturation vs. Distance (b). The Solid Curves in (a) Correspond to $G = 0$	44
Figure 12. Numerical (Dots) and Analytical (Line) Predictions of Threshold Permeabilities for Variable Pressure, Interfacial Tension, Residual Saturations and Thermal Conductivities.....	45
Figure 13. Solution Trajectories for the Geothermal Problem	

and $\epsilon = 0.0265275$: Temperature vs. Saturation (a) and Saturation vs. Distance (b). The Solid Curves in (a) Correspond to $G = 0$ 46

Figure 14. Solution Trajectories for the Geothermal Problem and $\epsilon = 0.0838876$: Temperature vs. Saturation (a) and Saturation vs. Distance (b). The Solid Curves in (a) Correspond to $G = 0$ 47

Figure 15. Solution Trajectories for the Geothermal Problem, with Heat Flux Exceeding the Limit (62): Temperature vs. Saturation. The Solid Curves Correspond to $G = 0$ 48

A STUDY OF STEADY-STATE STEAM-WATER COUNTERFLOW IN POROUS MEDIA

By

C. Satik, M. Parlur, and Y.C. Yortsos

ABSTRACT

Vapor-liquid counterflow in porous media arises in processes such as heat pipes, oil recovery and geothermal systems. Previous studies analysed these phenomena in separate contexts. This paper presents a unified description from which previous models result as limiting cases. The analysis includes capillarity, heat conduction, and Kelvin effects. The importance of each term to various processes is examined. Significantly, it is found that the critical heat flux is not constant but increases with decreasing permeability. A threshold permeability is identified below which steady states may not exist. Analogous conclusions are reached regarding liquid-dominated geothermal systems.

INTRODUCTION

The steady-state counterflow of a liquid and its vapor in porous media arises in many processes driven by temperature gradients. Large scale applications involve geothermal systems [1-4], thermal oil recovery [5], and nuclear waste disposal [6,7] among others. Investigations on the laboratory scale have emphasized porous heat pipes [8,9] and boiling processes [10-12]. All these studies share common aspects, principally the phase change and its interplay with fluid flow, heat transfer and capillarity.

Although change of fluid phase in porous media is fundamental to such routine applications as drying [13], a precise description of the process is not presently available. Issues of nucleation, stability of equilibrium states, supersaturation and heat and mass transfer are yet to be fully explored. Instead, the traditional approach is taken that vapor and liquid phases individually obey Darcy's law with saturation-dependent permeabilities.

Steady-state vapor-liquid flows in porous media have been modeled with such methodology for several decades [14]. Notable recent applications to steam-water counterflow include the works by Martin et al. [15], Schubert and Straus [16], Bau and Torrance [17], and Udell [18, 19]. The first two studies analyze the problem in the geothermal context, by neglecting capillarity, but including heat conduction. Udell [18, 19] considers the heat pipe version, in which capillarity predominates, but conduction is neglected. Finally, Bau and Torrance [17] present a simplified analysis where both conduction and capillarity are assumed negligible.

While previous studies have been instrumental in enhancing our understanding of the counterflow process, several areas are still obscure and in need of further in-

vestigation. In the context of a heat pipe, unresolved is the role of heat conduction, particularly as it regards the critical heat flux in bottom heating [17, 19]. The characterization of the flow regime for heat fluxes lower than the critical is also incomplete. The tacit, and unrealistic, assumption of an infinite, two-phase zone of constant saturation has not been questioned. Finally, unclear is the role and the importance of Kelvin effects in the process description. In the context of geothermal systems, the possible existence of two systems (vapor- and liquid-dominated) has long been proposed [15]. However, the question of selection of the particular regime also remains open.

The difficulty in obtaining answers to these questions is due to the approximations inherent to the various models, and the fact that they become singular in the region of interest. To alleviate this problem, a more detailed study is necessary. In recognition of the fact that all the above applications represent essentially the same problem (although temperature gradients, thus flow directions, may be of opposite sign), a common formalism should be possible. Specific cases should then arise in the appropriate limits. This forms the main objective of this paper. We shall consider a complete formulation that includes capillarity, heat conduction, phase change and vapor pressure lowering.

The flow model follows an extension of Darcy's law using relative permeabilities, and allows for vapor pressure lowering due to Kelvin effects. Both representations are based on the premise of capillary control at the pore level, usually enforced for low values of capillary and Bond numbers, and when temperature gradients are relatively low. Implicit is also the assumption that pore wall curvature stabilizes vapor-liquid interfaces. Such conditions are necessary for a process description in terms of saturation-dependent relative permeabilities and capillary pressure functions. Precise criteria for their validity are currently under development, paralleling recent advances in the related problem of bubble growth in porous media by diffusion [20], where such

and other issues have been addressed.

We proceed by deriving a dimensionless representation applicable to a general steady-state, vapor-liquid counterflow. The heat pipe and geothermal problems are subsequently analysed in separate sections. We investigate boundary layers due to vapor pressure lowering and heat conduction in the first case, and due to capillarity in the latter. The nature of the critical heat flux for bottom heating in a heat pipe problem, and its dependence on process parameters are examined in detail. Finally, for both heat pipe and geothermal problems we identify regimes, where steady-state counterflow may not exist.

FORMULATION

We consider the steady state, countercurrent flow of a single component, two-phase, liquid-vapor (e.g. steam-water) system. As a result of an externally imposed heat flux q_h , three regions develop [18]: Two no-flow regions (I or III in Fig. 1) containing mostly vapor or liquid, respectively, and an intermediate two-phase region (II), where counterflow occurs. In our notation, the space coordinate x increases in the direction from the liquid to the vapor. The system is inclined at an angle θ with respect to the horizontal, such that when $0 < \theta < \pi$ vapor is at the top, while the vapor zone is at the bottom in the other case ($\pi < \theta < 2\pi$).

Application of a momentum balance to the fluid phases gives

$$V_{Lx} = -\frac{k}{\mu_L} k_{rL} \left(\frac{\partial P_L}{\partial x} + \rho_L g \sin \theta \right) \quad (1)$$

$$V_{Vx} = -\frac{k}{\mu_V} k_{rV} \left(\frac{\partial P_V}{\partial x} + \rho_V g \sin \theta \right) \quad (2)$$

where the relative permeabilities k_{rL} and k_{rV} depend on the liquid saturation, S . This

formulation ignores viscous coupling between the two phases [21]. The two pressures are related via the capillary pressure function

$$P_V - P_L = P_c(S) = \frac{\sigma}{\sqrt{k}} J(S) \quad (3)$$

where the typical representation in terms of a Leverett J function was introduced.

Permeability and capillary pressure functions are controlled by pore space geometry and topology. Typical schematics are shown in Figure 2. The residual saturation values (S_{Lr}, S_{Vr}), below which flow of the respective phases ceases, should be noted. Significantly, and contrary to non-condensing phases, however, the capillary pressure is not singular at the residual values. Salient features of such properties for vapor-liquid systems are discussed elsewhere, following a percolation approach [20], [22]. In the ensuing use will be made of simple, although ad hoc, numerical expressions.

For the vapor pressure we take

$$P_V = P_{V_o}(T) \exp\left(-\frac{v_L}{RT} P_c(S)\right) \quad (4)$$

to describe pressure lowering, and use the Clausius-Clapeyron formula

$$P_{V_o}(T) = P_{V_o}(T_o) \exp\left(\frac{L_v M}{R} \left(\frac{1}{T_o} - \frac{1}{T}\right)\right) \quad (5)$$

for phase equilibria. Mass and thermal energy balances complete the formulation

$$\rho_L V_{Lx} + \rho_V V_{Vx} = 0 \quad (6)$$

$$\rho_V L_V V_{Vx} + q_h = \lambda \frac{\partial T}{\partial x} \quad (7)$$

To avoid unnecessary complications, all fluid properties are taken independent of P and T. Due to different flow behavior the various regimes are examined separately.

(i) No-Flow Regions

Region I is a no-flow, mostly vapor-occupied zone, where

$$0 \leq S \leq S_{Lr} \quad (8)$$

thus $k_{rL}(S) = 0$, $V_{Lx} = 0$ and, from (6), $V_{Vx} = 0$. At the residual value S_{Lr} , bulk liquid in the pore space becomes disconnected, and bulk flow ceases. The liquid being strongly wetting keeps hydraulic continuity in the form of thin film flow, even for $S < S_{Lr}$. These rates are quite low, however, and will not be considered here. Thus, the pressure of the vapor phase is hydrostatic and the temperature distribution linear

$$P_V = P_I - \rho_V g x \sin \theta \quad (9)$$

$$T = T_I + \lambda_I q_h x \quad (10)$$

where P_I, T_I are constants. A saturation profile results

$$J(S) = \frac{1}{b} \ln \left(\frac{P_{Vo}(T_I + \lambda_I q_h x)}{P_I - \rho_V g x \sin \theta} \right) \quad (11)$$

where the dimensionless group $b = \sigma v_L / RT \sqrt{k}$ parametrizes Kelvin effects. For media of practical interest ($b \ll 1$), the liquid is at low saturation ($J(S) \gg 1$) in most of region I, and exists in a pendular state. Recent works [23] have thoroughly elucidated the capillary pressure- saturation relationship in this regime. The extent (x_1) of the vapor zone I is demarkated by setting $S = S_{Lr}$ in (11). For $b \ll 1$, one may approximate

$$P_{Vo}(T_I + \lambda_I q_h x_1) \simeq P_I - \rho_V g x_1 \sin \theta \quad (12)$$

which is the condition for vapor saturation, and determines the boundary of the two regions I, II. The sharp saturation rise to the residual value S_{Lr} near the boundary (where the logarithm in (11) becomes of order b) should be noted.

Likewise, region III is a no-flow, mostly liquid-occupied zone, where

$$1 - S_{Vr} \leq S \leq 1 \quad (13)$$

thus, $k_{rV}(S) = 0$, $V_{Vx} = 0$, and, from (7), $V_{Lx} = 0$. Pressure and temperature profiles are linear

$$P_L = P_{III} - \rho_L g x \sin \theta \quad (14)$$

$$T = T_{III} + \lambda_{III} q_h x \quad (15)$$

with P_{III}, T_{III} appropriate constants. In contrast to region I, where a saturation profile exists due to wettability, the bulk of region III (IIIb in Figure 1) is at $S = 1$. Saturation changes are confined within a narrow sub-domain (IIIa), the boundary of which (x_3) is the solution of $P_c = 0$

$$P_{Vo}(T_{III} + \lambda_{III} q_h x_3) = P_{III} - \rho_L g x_3 \sin \theta \quad (16)$$

To the left lies boundary x_2 , obtained by taking $S = 1 - S_{Vr}$, and by neglecting the Kelvin effect

$$P_{Vo}(T_{III} + \lambda_{III} q_h x_2) = P_{III} - \rho_L g x_2 \sin \theta + \frac{\sigma}{\sqrt{k}} J(1 - S_{Vr}) \quad (17)$$

(ii) Flow Region

The region of two-phase, countercurrent flow is the most interesting. It is here, where condensation and evaporation occur, and where the interplay between phase change, heat transfer and capillarity is most pronounced. Saturation and temperature profiles are described by two coupled equations obtained by combining (1)-(7). After considerable algebra the following system is obtained

$$\frac{d\tau}{d\xi} = \frac{H(\tau, S)}{F(\tau, S)} \quad (18)$$

$$\frac{dS}{d\xi} = \frac{G(\tau, S)}{F(\tau, S) \frac{dJ}{dS}} \quad (19)$$

where

$$H = k_{rL}[(1 + bR_p A)R_h + \sin \theta k_{rV}(bR_m A - R_v R_c)] + bk_{rV}\beta R_p R_h A \quad (20)$$

$$F = k_{rL}[1 + bR_p A + k_{rV}KR_m \frac{A}{\tau^2}] + bk_{rV}\beta R_p A \quad (21)$$

$$G = k_{rL}[\sin \theta R_l + KR_p R_h \frac{A}{\tau^2} + \sin \theta k_{rV}KR_m \frac{A}{\tau^2}] + \beta k_{rV}[\sin \theta R_v + KR_p R_h \frac{A}{\tau^2}] \quad (22)$$

Dimensionless notation has been used, with ξ denoting distance normalized by $\sigma/\sqrt{k}g\Delta\rho$, to reflect competition between gravity and capillarity, and τ denoting temperature normalized by a suitably chosen temperature T_o . Variable A is a vapor pressure normalized by the saturation pressure at T_o and includes Kelvin effects

$$A = \exp\left(K\left(1 - \frac{1}{\tau}\right) - bJ(S)\right) \quad (23)$$

The various dimensionless groups are defined in the Nomenclature and they are functions of the fluid and rock properties, with the exception of R_h

$$R_h = \frac{q_h \sigma}{\lambda_{II} T_o \sqrt{k} g \Delta \rho} \quad (24)$$

which is a measure of the imposed heat flux, and is simply related to the parameters ω or Γ [18], [16]

$$\omega = \frac{R_p R_h}{R_m} = \frac{\lambda_{II} \Gamma \mu_V}{k L_V g \Delta \rho \rho_V} \quad (25)$$

The above constitute an initial value problem to be solved subject to appropriate initial conditions. For the heat pipe problem [18] we shall take

$$\tau = \frac{T_1}{T_o} \quad ; \quad S = S_{Lr} \quad \text{at} \quad \xi = \xi_1 \quad (26)$$

where $T_1 = T_o + \lambda_I q_h x_1$, the reference temperature T_o corresponds to the (dry) end of the vapor zone, and the integration is in the direction of decreasing ξ . For the geothermal problem [16] we shall consider

$$\tau = 1 \quad ; \quad S = 1 \quad \text{at} \quad \xi = 0 \quad (27)$$

where T_o corresponds to the boundary of regions IIIa-IIIb, and the integration is in the direction of increasing ξ . Forward integration of (18) and (19) subject to (26) and (27) uniquely determines saturation and temperature profiles.

For future reference the dimensionless vapor flow velocity V_{Vx} , normalized by $k\Delta\rho g/\mu_V$, is also derived

$$V_{Vx} = - \frac{k_{rV} k_{rL} [\sin \theta R_v - b R_p A + K R_p R_h \frac{A}{\tau^2}]}{F(\tau, S)} \quad (28)$$

It must be remarked that, for all practical purposes ($b \ll 1$), the magnitude, but not the sign, of the angle θ can be scaled out in (18), (19), and (28), by rescaling the space variable ξ by $|\sin \theta|$ and the heat flux term R_h (or ω) by $1/|\sin \theta|$. Thus, it only suffices to study the generic cases $\theta = \pi/2, 3\pi/2$.

Contrasted to the above, and excluding field-scale numerical simulators, present models are quite simpler. The most advanced belongs to Udell [18, 19], for the heat pipe and to Schubert and Straus [16], for the geothermal problem. These models arise as limiting cases of the above formulation as will be shown below. To facilitate the presentation, however, the two cases are examined separately.

I. HEAT PIPE PROBLEM

In the context of the heat pipe problem we shall investigate Kelvin and heat conduction effects, and will explore the critical heat flux curve. For this purpose,

we will frequently refer to the model in [18], [19], the corresponding temperature, saturation and vapor flux of which will be denoted by Θ , Σ , and Ψ , respectively. In our notation, the analysis in [18], [19] is tantamount to taking $b \ll 1$, and $K R_m \gg 1$ with R_h/R_m fixed, the latter condition corresponding to negligible heat conduction. Indeed, at these limits, the vapor flow rate (28) reduces to

$$V_{V_x} \longrightarrow \Psi = \omega \quad (29)$$

and the saturation eqn (19) becomes uncoupled from temperature

$$J' \frac{d\Sigma}{d\xi} = \sin \theta + \omega \left(\frac{1}{k_{rV}} + \frac{\beta}{k_{rL}} \right) \quad (30)$$

The above two limits delineate the validity of the previous results. The condition for negligible Kelvin effects, $b \ll 1$, is generally well satisfied for most porous media of practical interest (e.g. permeabilities exceeding $O(\text{md})$). Neglecting heat conduction, on the other hand, requires $K R_m \gg 1$ at fixed R_h/R_m , a significantly tighter restriction (e.g. $k \gg O(100 \text{ md})$ for the experiment in [18]). Substantial changes may result when this condition is not satisfied, as shown in the next section.

Boundary Layer Analysis

As a consequence of the conditions $b \ll 1$, $1/K R_m \ll 1$ two boundary layers arise at the ends of region II. This is evident from (29) which requires a step change in the vapor flux, thus infinitely large evaporation-condensation rates at the boundaries. In actuality, however, the vapor flux vanishes smoothly at the two boundaries (where the two relative permeabilities also vanish), as can be seen from an expansion of the full expression (28)

$$V_{V_x} \sim \begin{cases} -\frac{k_{rL} K R_h}{b \beta \tau^2} & ; \quad S \rightarrow S_{Lr} \\ -\frac{k_{rV} K R_p R_h A}{\tau^2} & ; \quad S \rightarrow 1 - S_{vr} \end{cases} \quad (31)$$

We analyse the solution in the two regions by considering the more general case $b \ll 1$, finite $K R_m$, which is widely applicable to a large class of porous media.

(i) Case $b \ll 1$, Finite $K R_m$

Here, the outer solution outside the boundary layer (superscript (o)) is obtained by neglecting Kelvin effects in (18), (19) and (28)

$$\frac{d\tau^{(o)}}{d\xi} = \frac{R_h - k_{rV} R_v R_c}{1 + k_{rV} \frac{K R_m A}{(\tau^{(o)})^2}} \quad (32)$$

$$\frac{dS^{(o)}}{d\xi} = \frac{G(\tau^{(o)}, S^{(o)})}{k_{rL} \left(1 + k_{rV} \frac{K R_m A}{(\tau^{(o)})^2}\right) J'(S^{(o)})} \quad (33)$$

$$V_{V_x}^{(o)} = - \frac{\sin \theta k_{rV} \left[R_v + K R_p R_h \frac{A}{(\tau^{(o)})^2} \right]}{1 + k_{rV} \frac{K R_m A}{(\tau^{(o)})^2}} \quad (34)$$

Near S_{Lr} the saturation (although not the temperature) gradient diverges, thus a saturation rescaling is needed. We take the typical expansion, $k_{rL} \sim L(S - S_{Lr})^n$, where $L > 0$ is constant and $n > 1$, and rescale

$$S = S_{Lr} + b^\alpha \sigma(z) \quad (35)$$

$$\xi = \xi_1 - b^\kappa z \quad (36)$$

with $\alpha, \kappa > 0$ to be determined. Substitution into the full equations (18) and (19), subsequent expansion and use of dominant balance [24], results into

$$\alpha = \frac{1}{n} \quad (37)$$

$$\kappa = 1 + \frac{1}{n} \quad (38)$$

One immediately concludes that the (evaporation) boundary layer is of the order $b^{1 + \frac{1}{n}}$. The corresponding vapor flux in the boundary layer is obtained from (28)

$$V_{V_x} = \frac{V_{V_x}^{(o)}(S_{Lr})}{1 + c \sigma^{-n}} \quad (39)$$

It correctly predicts the vanishing of V_{V_x} at the one end ($\sigma = 0$) and the asymptotic approach to the outer value, $V_{V_x}^{(o)}(S_{Lr})$, at the other ($\sigma \rightarrow \infty$) (Figure 3a). In turn, the saturation profile can be also constructed

$$\sigma + \frac{\sigma^{n+1}}{(n+1)c} = -ez \quad (40)$$

thus, the dimensionless evaporation rate $\dot{m} = \frac{dV_{V_x}}{d\xi}$ can be evaluated

$$\dot{m} = \frac{f \sigma^{n-1}}{b^{1+\frac{1}{n}} [1 + \frac{\sigma^n}{c}]^3} \quad (41)$$

where c , e and f are process constants (Appendix). A normalized plot is shown in Figure 3b. It is noted that all evaporation takes place within the boundary layer, \dot{m} increasing from zero to a maximum value, before rapidly decaying to zero at the end of the boundary layer ($z \rightarrow +\infty$). The local rates intensify for smaller values of b , for example when the permeability increases, such that the total evaporation rate over the layer remains finite

$$I = \int_0^{+\infty} b^{1 + \frac{1}{n}} \dot{m} dz = -\frac{fc}{en} \quad (42)$$

Of course, the latter equals the jump in the outer value $V_{V_x}^{(o)}(S_{Lr})$, which is discontinuous at S_{V_r} .

The above analysis shows that the evaporation region is a thin layer of order $b^{1 + \frac{1}{n}}$ at the interface between dry and two-phase zones, and is principally controlled by vapor pressure lowering. Outside this layer in region II, Kelvin effects are insignificant, regardless of the value of KR_m , and the process is well described

by the outer solutions (18), (32) and (34). In particular, the latter shows that the vapor flux magnitude $|V_{Vx}|$ continuously decreases, as S increases, suggesting that condensation occurs over the entire two-phase zone, and not strictly at the end as normally assumed. On the other hand, local condensation rates depend on the value of KR_m . For large values of the latter, as implicitly taken in [18, 19], condensation is restricted on a boundary layer at the interface between liquid and two-phase zones. This boundary layer is due to heat conduction alone.

(ii) Case $b \ll 1$, $KR_m \gg 1$, R_h/R_m Finite

In this limit, the outer solutions (Θ , Σ and Ψ) are given by expressions (29) and (30) and

$$R_p \frac{d\Theta}{d\xi} = \frac{\omega - k_{rV} R_v}{\frac{KA}{\Theta^2} k_{rV}} \quad (43)$$

Under the tacit, and sufficient, assumption $b \ll \delta \equiv 1/KR_m$, the previous analysis is valid, and only the boundary layer near $1 - S_{Vr}$ needs be considered. Now, however, the temperature gradient also diverges. To proceed, we first note that to first-order the boundary temperature at ξ_2 is given by the outer solution by combining (33) and (43) and integrating across the two-phase zone

$$R_p(A_2 - A_1) = \omega \int_{S_{Lr}}^{1-S_{Vr}} \frac{J'(S)dS}{k_{rV}[\sin \theta + \omega(\frac{1}{k_{rV}} + \frac{\beta}{k_{rL}})]} \quad (44)$$

Here $A = \exp[K(1 - \frac{1}{\Theta})]$ and it was implied that the denominator does not vanish (see also below). Next, we rescale saturation, spatial distance and temperature as before

$$S = 1 - S_{Vr} - \delta^\alpha \sigma(z) \quad (45)$$

$$\xi - \xi_2 = \delta^\alpha z \quad (46)$$

$$\Theta = \Theta_2 + \delta^\gamma \eta(z) \quad (47)$$

to obtain with the use of dominant balance

$$\alpha = \gamma = \frac{1}{m} \quad (48)$$

$$\kappa = 1 + \frac{1}{m} \quad (49)$$

where m is the exponent in the permeability expansion $k_{rV} \sim M(1 - S - S_{Vr})^m$. The rescaled saturation satisfies the equation

$$\frac{d\sigma}{dz} = -\frac{\omega G}{J'(1 - S_{Vr})[1 + MG\sigma^m]} \quad (50)$$

where $G = A_2/\Theta_2^2$. An analysis similar to the previous applies, and identical results can be reached regarding condensation rates. For example, the vapor flux inside the boundary layer has the form

$$V_{Vx}^{(o)} = -\frac{\omega}{1 + \frac{\sigma^{-m}}{LG}} \quad (51)$$

which correctly predicts that V_{Vx} vanishes at $1 - S_{Vr}$ ($\sigma = 0$) and approaches the asymptotic value $-\omega$ in the outer limit ($\sigma \rightarrow \infty$). We omit further details and only mention that both the boundary location and the boundary temperature are accurately approximated at large KR_m from the outer solutions. At such conditions, vapor condensation is restricted in a boundary layer of width $\delta^{1+\frac{1}{m}}$ at the end of the two-phase zone, and the temperature drop across the two-phase region is given by (44), which reflects solely the interaction between capillarity and phase change.

We conclude that in the general case of practical interest, evaporation occurs only within a boundary layer in the vicinity of the vapor zone, outside of which vapor pressure lowering due to Kelvin effects can be safely neglected. By contrast, condensation is driven by heat conduction and, unless $\delta = 1/KR_m \ll 1$, it may not be neglected in the bulk of the two-phase zone. It is expected that in several practical applications KR_m is not necessarily large, thus previous results [17-19] may

be inapplicable. The effect is most significant in the estimation of the critical heat flux.

Critical Heat Flux

To proceed, a numerical scheme based on stiff ODE solvers was used, the integration starting from region I and consecutively marching through regions II and III. Standard runs were carried out at the conditions of Table 1. An illustration of the applicability of the scheme is shown in Figure 4, where temperature and saturation profiles corresponding to the experiment in [18] ($\theta = \pi/2$, $b = 0.0001346$, $KR_m = 5184.033$) are plotted. An excellent match is obtained between experimental and theoretical predictions for the temperature profile. Lack of data for saturation does not permit an assesment of the functional forms used for relative permeabilities and capillary pressure. However, the plot exhibits the expected salient boundary layer features (it must be noted that $P_c(0)$ is finite in the present model).

Subsequently, a systematic numerical study was undertaken. In general, results consistent with [18, 19] were obtained in the limit of large KR_m . For example, in the more interesting case of bottom heating [19], critical heat flux values ω_{cr} were found, such that for $\omega/(-\sin\theta) > \omega_{cr}$ a two-phase zone exists of a length that decreases as ω increases. This behavior was thoroughly analysed previously [19]. Unexplored in past investigations, however, were the effects of KR_m and the nature of the solution for $\omega < \omega_{cr}$.

While at large KR_m (or k) the critical flux was indeed found to approach the asymptote [19]

$$\omega_{cr} = (-\sin\theta) \max_S \left\{ \frac{k_{rL}k_{rV}}{(k_{rL} + \beta k_{rV})} \right\} \quad (52)$$

which is largely independent of process parameters, it was also found that ω_{cr} slowly

increases with decreasing KR_m (or k), and rapidly diverges when a critical permeability value k_b is approached (Figure 5). This singular behavior was verified for a host of parameter values, the standard case yielding the estimate $k_b = 144$ md, well within the range of natural reservoir rocks.

This interesting feature has not been noted before and may lead to significant implications. Given a process, a critical value k_b can be demarkated such that steady-state solutions are possible for $k > k_b$, in which case a minimum heat flux is required (region A in Fig. 5). The magnitude of the latter is not constant, although it approaches at large k the no-conduction asymptote (52). In the opposite case, $\omega < \omega_{cr}$ or $k < k_b$, saturation and temperature profiles are ill-behaved, in a manner to be precisely specified below, and the existence of steady-state solutions must be seriously questioned.

The sensitivity of k_b was subsequently investigated. Thermal conductivity was found to have no effect on k_b , although it significantly influences the shape and magnitude of the critical curve. A sensitivity, generally weak, was observed upon an increase in the residual saturations (which lead to a decrease of the overall permeabilities in the model of Table 1), the trend being a somewhat higher threshold k_b at lower residual saturations.

Most significant were the effects of capillarity and the imposed pressure P_o (Fig. 6). In both cases, the threshold value varied significantly, roughly in proportion to the square of σ/P_o . While substantial changes in σ mainly require changes in the fluid chemistry, large variations in P_o can be accomplished with relative ease. Therefore, a wide variation in k_b is possible. For the typical conditions of previous laboratory experiments, relatively high thresholds should be expected. By contrast, k_b values of $O(\mu\text{d})$ would be obtained in typical geothermal systems involving large pressures.

An interpretation of the critical permeability value is offered in the following. Prior to this, numerical results for top heating are also presented. As expected, no constraint in the process parameters exists at large KR_m . At smaller permeability values, however, a sensitivity similar to the previous was detected and a similar (although not as sharp) threshold k_t was identified. Now, steady-states are possible for any heat flux value, if $k > k_t$, and for sufficiently low heat flux values, $\omega < \omega_{cr}$ if $k < k_t$ (region A in Fig. 7). In the opposite case (B in Fig. 7), a steady-state counterflow may not be sustained. Sensitivity studies revealed features similar to the case of bottom heating. Capillarity and imposed pressure P_o were found to be the most important variables. In fact, the two thresholds k_t and k_b were found to practically coincide.

A pictorial schematic of the above is shown in Fig. 8, where the composite of the critical heat flux ω_{cr} near the critical region was constructed. For the case of top heating ($0 < \theta < \pi$), steady-state solutions are possible within the "tunnel" at the front-left, the cross section of which expands to an infinitely large value when $k > k_b$. Conversely, in the case of bottom heating ($\pi < \theta < 2\pi$), steady-states can be sustained only outside the "tunnel" at the back-right, the cross-section of which also diverges when $k < k_b$.

To analyze the critical heat flux curve, the nature of the solution for $\omega < \omega_{cr}$ must be examined. We consider a representative example of bottom heating, with $k=1d$ and parameter values $S_{Lr} = S_{Vr} = 0$. Here the critical heat flux is $\omega_{cr} = 0.45$, a significantly larger value than 0.306348 obtained from the estimate (52). A sequence of (τ, S) and (ξ, S) trajectories are shown in Figures 9-11 for the values $\omega = 0.1, 0.4$, and 0.5, respectively. Plotted also are the level curves when the numerator in (19) vanishes, $G(\tau, S) = 0$, a condition necessary for the change of slope in the (τ, S) trajectory.

The first case (Figure 9) is characteristic of one kind of ill-condition, namely the domain $G > 0$ is disconnected and does not extend over the entire saturation interval. As a result, the solution trajectory changes slope at some point (A in Fig. 9), and further penetration into the two-phase region leads to progressively higher steam saturation and unphysically low temperatures. Previous investigators [17], [19] have speculated that a two-phase zone of “infinite” length would develop under such conditions. While it is true that penetration depth for a given saturation is significantly higher (Figure 9), and in fact it should increase even more as KR_m increases (both the trajectory and the $G = 0$ level curve becoming steeper in the latter case), our results show that unrealistically low temperatures and vapor pressures are eventually reached and the two-phase zone terminates at non-physical values. We argue against the existence of a steady-state under such conditions.

The second case (Figure 10) is characteristic of a different kind of ill-condition. Although the domain $G > 0$ spans the entire saturation interval $(0, 1)$, the value of ω is not high enough, thus the (τ, S) trajectory intersects the $G = 0$ curve before it reaches the end of the two-phase zone. This condition is entirely due to the finite value in KR_m , the no-conduction model predicting no pathological behavior for $\omega > 0.306348$, as pointed out above. By contrast, at the point of intersection A, the saturation profile exhibits a turning point and the ill-condition of the previous case is encountered. For sufficiently large values of ω , however, the two curves are at large enough distance, such that the solution trajectory terminates at the end of the two-phase zone before intersection, and a true heat pipe is established (Fig. 11). Smaller values in k lead to increasingly larger critical heat flux values and, at least within a certain range of k away from k_b , the above interpretation of the ω_{cr} vs k curve applies.

While the departure of ω_{cr} from the asymptote (52) was attributed primarily to conduction, near the critical region ($k \sim k_b$) capillarity becomes predominant. The condition determining ω_{cr} still remains the same, namely that a turning point in the

saturation profile develops. It was numerically observed that here, the latter occurs at the end of the two-phase zone, where $S \rightarrow 1 - S_{vr}$ and $k_{rV} \rightarrow 0$. Substitution in $G = 0$, then yields

$$\frac{\omega_{cr}}{-\sin \theta} \simeq \frac{1}{KR_m} \left(\frac{\tau^2}{A} \right)_2 \gg 1 \quad (53)$$

The novel feature, however, is that now ω_{cr} becomes infinitely large as k approaches k_b , which in view of the finite value of KR_m must be attributed to the vanishing of the vapor pressure A_2 . An estimate of the latter can be obtained from (18) and (19) by taking the large ω limit

$$R_p \frac{KA}{\tau^2} \frac{d\tau}{dS} = \frac{dJ}{dS} \frac{k_{rL}}{(k_{rL} + \beta k_{rV})} \quad (54)$$

which is further integrated to

$$R_p(A_2 - A_1) \simeq \int_{S_{Lr}}^{1-S_{vr}} \frac{k_{rL} J'(S) dS}{(k_{rL} + \beta k_{rV})} \quad (55)$$

Expectedly, this is also the limit of (44) for the case of horizontal heating. Thus, the critical threshold k_b can be determined in the limit $A_2 \ll 1$

$$k_b \simeq \left(\frac{\sigma}{P_o} \right)^2 \left[\int_{S_{Lr}}^{1-S_{vr}} \left(-\frac{dJ}{dS} \right) \frac{k_{rL} dS}{(k_{rL} + \beta k_{rV})} \right]^2 \quad (56)$$

The above contains all essential features of the threshold value numerically observed, notably the square dependence on the ratio σ/P_o and the weaker effect of relative permeabilities. The agreement between numerical and analytical results is excellent, as illustrated in Figure 12. After additional algebra, an estimate of the critical curve near k_b may be also derived

$$\frac{\omega_{cr}}{-\sin \theta} \sim \frac{(\text{const})}{KR_m (k - k_b) (\ln |k - k_b|)^2} \quad (57)$$

The latter contains through R_m the numerically observed effect of λ . As noted, conductivity does not affect the threshold value, although it influences the shape of the critical curve.

Identical considerations apply for the case of top heating. The onset of critical behavior was numerically found to coincide with unphysically low temperatures, first encountered at the end of the two-phase region. In the limit $1 \ll \omega < \omega_{cr}$ it is easily shown that the previous analysis holds identically.

To provide a more physical understanding, we first consider the horizontal case, $\theta = 0$. For negligible Kelvin and other secondary effects, the two-phase flow region starts when the vapor becomes saturated, $P_V = P_o$. Counterflow in this region is possible only because of capillarity. In fact, the changes in vapor pressure and capillary pressure are interrelated

$$dP_V = \frac{k_{rL}}{k_{rL} + \beta k_{rV}} dP_c \quad (58)$$

As long as capillarity is not strong, the vapor pressure drop across the region is not large

$$P_V = P_o - \int_0^{P_c(S_{Lr})} \frac{k_{rL}}{k_{rL} + \beta k_{rV}} dP_c \quad (59)$$

and $P_V > 0$. Problems arise when the permeability is low, such that capillarity is large enough for the RHS to become negative. It is straightforward to show that the onset of this condition occurs at the above threshold, k_b . Below this value, capillarity imposes large pressure drops, thus negative values for P_V result with catastrophic consequences on the temperature profile. Clearly, k_b (or k_t) also denotes the lowest permeability value below which steady-state, horizontal counterflow cannot be sustained.

When the medium is inclined, gravity opposes or supplements capillary action, depending on whether the vapor overlies or underlies the liquid. For instance, the expression equivalent to (59) is

$$P_V = P_o - \int_0^{P_c(S_{Lr})} \frac{k_{rL}}{k_{rL} + \beta k_{rV}} dP_c + \rho_L g \sin \theta \int_{x_2}^{x_1} I dx \quad (60)$$

where

$$I = \frac{k_{rL} + \beta R_v k_{rV}}{k_{rL} + \beta k_{rV}} \quad (61)$$

When heating is from the top, capillary pressure is counterbalanced by adverse gravity effects, and a two-phase region may exist even for $k < k_t$, provided that the heat flux is small enough. For this, it is recalled that the extent of the two-phase zone increases as the heat flux decreases. Certainly, heat transfer is of importance here. Opposite considerations apply for the case of bottom heating. At least near k_b , gravity would supplement capillarity in increasing pressure drops, with a contribution roughly proportional to the extent of the two-phase zone. At low $\omega < \omega_{cr}$, the latter is large enough and a steady-state cannot be sustained.

One concludes that consideration of conduction and lower permeability values in the heat pipe problem leads to unexpected, non-trivial corrections, particularly for the case of bottom heating. The relevance of the threshold k_b to heat pipe problems cannot be discounted. A possible distinction from the geothermal problem to be discussed in the following, is the emphasis on capillarity, a measure of which is the parameter R_p . For values of the latter of $O(1)$ or less, the corresponding k_b value would be of the same order with the medium permeability (compare eq.(56)), and the regimes analysed above are likely to be encountered in a heat pipe problem.

II GEOTHERMAL PROBLEM

The next part of this paper addresses the geothermal version of the steady-state, vapor-liquid counterflow, specifically the problem considered by Martin et al. [15] and Schubert and Straus [16] among others. Here $0 < \theta < \pi$, but the heating is from the bottom, namely the imposed temperature gradient and heat flux are negative (in the direction from the liquid to the vapor). As noted before, we shall take reference values corresponding to the liquid- two-phase zone interface, where for simplicity the value $S_{V,r} = 0$ will be assumed. Integration proceeds in the positive ξ direction, from

the liquid towards the vapor. The condition derived in [16] is also recalled that the underlying liquid is subcooled, hence the temperature gradient or the heat flux may not exceed an upper limit. In our notation one obtains

$$-\omega < \frac{R_l}{KR_m} \sim \frac{1}{KR_m} \quad (62)$$

To obtain the geothermal problem from the original formulation (18)-(22), the following limit is considered in the absence of Kelvin effects

$$KR_p \gg 1 \quad (63)$$

With reference conditions corresponding to the top of the liquid zone the above reads in dimensional notation

$$\frac{L_v P_o M_w}{RT_o} \gg \frac{\sigma}{\sqrt{k}} \quad (64)$$

Consistent with [15, 16] conditions (63) or (64) imply that capillarity is of secondary importance and sharply differentiate geothermal and heat pipe problems. To proceed we utilize (63) in (18)-(22) and obtain

$$\frac{d\tau}{dS} = -\epsilon \frac{k_{rL}[KR_m(-\omega) + KR_m R_v k_{rV}] \frac{dJ}{dS}}{G(\tau, S)} \quad (65)$$

$$\frac{dS}{d\xi} = \frac{G(\tau, S)}{k_{rL}[1 + KR_m \frac{A}{\tau^2} k_{rV}] \frac{dJ}{dS}} \quad (66)$$

where we denoted $\epsilon = 1/KR_p$ and

$$G(\tau, S) = k_{rL}[R_l + KR_m \omega \frac{A}{\tau^2} + KR_m \frac{A}{\tau^2} k_{rV}] + \beta k_{rV}[R_v + KR_m \omega \frac{A}{\tau^2}] \quad (67)$$

In general, G and $KR_m \omega$ are of $O(1)$ or less (compare with (62)). Thus, in the geothermal limit $\epsilon \ll 1$, solution trajectories (τ, S) have constant temperature, in regions where G is not small, and closely follow the $G = 0$ curve, otherwise (Figure 13a). In the region of constant temperature, the saturation changes rapidly over an interval of $O(1)$ in length (which, as recalled, expresses a balance between gravity and capillarity in the present notation). It is in this region, where capillarity influences

the saturation profile, and which was considered a sharp interface in the previous works [15, 16].

Significant temperature changes start occurring when the solution trajectory approaches the curve $G(\tau, S) = 0$. For the conditions of Figure 13, the latter is precisely the vapor-dominated limit analysed by Schubert and Straus [16] for a simpler model with straight-line relative permeabilities. As is apparent from (66), the saturation gradient is very small ($G \ll 1$) in this domain, thus, the extent of the region is quite large (Fig. 13b). In the limit $\epsilon \ll 1$, the region commences at saturation S^* satisfying $G(1, S^*) = 0$, a condition previously derived in different notation [16]. At larger values of ϵ , capillarity can become important and must be also considered (Fig. 14). Here, although ultimately attracted to the curve $G(\tau, S) = 0$, the solution trajectory shows substantial temperature variation before the vapor-dominated region is entered.

With an approximation that rapidly improves as ϵ diminishes, the previous analysis [16] describes the behavior of steam-water counterflow in the geothermal context with excellent accuracy. Considerations similar to [16] were also advanced by Martin et al. in an earlier publication [15]. While identifying the vapor-dominated regime, Martin et al. additionally proposed the existence of liquid-dominated regions. The present formulation readily yields such solutions as well. For this, it is required that the equation $G(1, S^*) = 0$ admits two solutions, a condition demanding higher values in ω .

At such conditions, the (τ, S) diagram is divided into three regions (two far regions with $G < 0$ and a middle one with $G > 0$) by the two branches of the curve $G = 0$ (Figure 15). In the present context, the proposed theory [15] can then be interpreted as follows: Vapor- or liquid- dominated regimes commence at points A or B, respectively, where $G(1, S^*) = 0$, and they subsequently follow the respective branches of $G(\tau, S) = 0$ (paths AV, BL, respectively). Such behavior appears consistent with

(65) and (66) in the limit $\epsilon \ll 1$, but it is doubtful that it actually materializes.

By definition, a solution trajectory must originate from the top of the liquid zone (point C, where $G < 0$), other starting conditions being impossible in a steady-state counterflow system. This trajectory has a negative slope and rapidly approaches the $G = 0$ branch to which it becomes parallel (dashed line path CD in Figure 15). Somewhat similar to the heat pipe problem (Figure 9), the solution trajectory crosses over to the middle region ($G > 0$), thus acquires positive slope and parallels the branch $G = 0$ from the other side (note that the two curves practically coincide in Figure 15).

While being different than that previously proposed (path BL), this solution is not acceptable either. An inspection of (66) reveals that ξ must decrease along the path CD, contradicting the requirement that, by convention, ξ increases in the direction from the “liquid” to the “vapor”. The other alternative, namely the trajectory extending from point C in the direction opposite to D, is also rejected as it leads to saturation values larger than one. It becomes evident that under such heat flux conditions a liquid-dominated regime is not realistic, while the vapor-dominated regime is never reached, certainly not when the starting point is the top of the liquid zone, as assumed throughout. One is led to conjecture that steady-state solutions are not possible for such cases, which require that the heat flux exceeds a certain value. The latter is easily determined to be the upper bound (62). The implied contradiction serves to reinforce the above conclusion.

A final remark is also appropriate regarding the analysis presented by Bau and Torrance [17]. These authors examine a configuration with $\theta = 3\pi/2$ and bottom heating (steam at the bottom, temperature gradient in the direction from the vapor to the liquid zone), a problem analyzed in the heat pipe section. In addition to conduction, however, they also neglect capillarity. Because of the latter, some

similarities with the geothermal problem may exist. In our formulation, their analysis corresponds to the conditions $KR_p \gg 1, KR_m \gg 1$. By simple rearrangement, equations (18)-(22) read for this problem

$$\frac{d\tau}{dS} = \epsilon \frac{k_{rL}(\omega + k_{rV}R_v) \frac{dJ}{dS}}{G(\tau, S) \frac{A}{\tau^2}} \quad (68)$$

$$\frac{dS}{d\xi} = \frac{G(\tau, S)}{k_{rL}k_{rV}} \frac{dS}{dJ} \quad (69)$$

where $\epsilon = 1/KR_p$ and

$$G(\tau, S) = (k_{rL} + \beta k_{rV})\omega - k_{rL}k_{rV} \quad (70)$$

It readily follows that despite the small capillary effects, the problem is of the same nature as that of the heat pipe thoroughly analysed before. Thus, identical conclusions must be reached regarding solution trajectories and the critical heat flux value, ω_{cr} , which is the necessary lower limit for the existence of a steady-state, steam-water counterflow. Under the implied assumption of negligible conduction, $KR_m \gg 1$, this critical value coincides with the asymptote (52).

CONCLUSIONS

In this paper we have attempted to unify the description of a diverse set of problems arising in heat pipe and geothermal contexts that contain the common mechanism of steady-state, vapor-liquid counterflow. The formalism introduced encompasses several previous studies, which arise as special cases at various limits. In particular, a quantitative assesment of the importance of gravity, capillarity, phase equilibria, heat conduction and Kelvin effects becomes possible.

In the context of the heat pipe problem, it was shown that Kelvin effects are of significance only over a narrow boundary layer at the vapor-two phase boundary,

and are otherwise negligible in the counterflow region. Heat conduction was found to influence saturation and temperature profiles near the other end of the two-phase region. It was conjectured that for the case of bottom heating, steady-state counterflow is not possible when the heat flux is below a critical value. Contrary to previous results, the latter is constant only in the limit of large permeability. A permeability threshold value k_b was identified, such that no steady-state counterflow can exist for media of lower permeability. The threshold reflects capillary effects and is mainly a function of the imposed pressure.

The geothermal problem was similarly analysed. The results of Schubert and Straus [16], where capillarity is neglected, were recovered as a limiting case of the present formulation. The same limit is also applicable for the cases discussed by Martin et al. [15]. However, the liquid-dominated regime suggested in the latter was found to lead to non-physical predictions, and it was suggested that such a steady-state may not be reached. It is hoped that the present analysis clarifies several of the issues involved in steady-state, vapor-liquid counterflow, and that it may be useful as a backbone for further studies in this area.

ACKNOWLEDGEMENT

This work was partly supported by DOE Contract DE-FG19-87BC14126, the contribution of which is gratefully acknowledged.

NOMENCLATURE

- A = Dimensionless vapor pressure.
 b = Dimensionless Kelvin group.
 g = Gravitational constant, $[LT^{-2}]$.
 J = Dimensionless capillary pressure.
 $K = (L_v M_w)/(T_o R)$, dimensionless.
 k = Permeability, $[L^2]$.
 L_v = Latent heat, $[L^2 T^{-2}]$.
 \dot{m} = Dimensionless evaporation rate.
 M_w = Molecular weight of water, $[Mmole^{-1}]$.
 n = Permeability exponent, dimensionless.
 P = Pressure, $[ML^{-1} T^{-2}]$.
 q_h = Heat flux, $[MT^{-3}]$.
 R = Gas constant, $[L^2 T^{-2} mole^{-1} K]$.
 $R_c = (k \rho_V L_v \sigma)/(\mu_V \sqrt{k} \lambda_{II} T_o)$, dimensionless.
 $R_h = (q_h \sigma)/(\lambda T_o \sqrt{k} g \Delta \rho)$, dimensionless.
 $R_i = \rho_L / \Delta \rho$, dimensionless.
 $R_m = (k L_v P_{V_o}(T_o) \rho_V)/(\mu_V \lambda_{II} T_o)$, dimensionless.
 $R_p = (P_{V_o}(T_o) \sqrt{k})/(\sigma)$, dimensionless.
 $R_v = \rho_V / \Delta \rho$, dimensionless.
 S = Saturation, dimensionless.
 T = Temperature, $[K]$.
 V = Volumetric flow rate, $[LT^{-1}]$

Greek letters :

- $\epsilon = 1/K R_p$, dimensionless.
 θ = Angle of inclination, degree.
 λ = Thermal conductivity, $[MLT^{-3} K^{-1}]$.
 μ = Viscosity, $[ML^{-1} T^{-1}]$.
 ξ = Dimensionless distance.
 ρ = Density, $[ML^{-3}]$.
 σ = Surface tension, $[MT^{-2}]$.
 τ = Temperature, dimensionless.
 v_L = Liquid molar volume, $[L^3 mole^{-1}]$.
 ω = Heat flux, dimensionless.
 Γ = Temperature gradient, $[KL^{-1}]$.
 $\Delta \rho = \rho_L - \rho_V$, $[ML^{-3}]$.

Subscripts :

b= Threshold

c= Capillary

cr= Critical

L= Liquid

o= Reference

r= Relative

V= Vapor

Vo= Saturation

I= Region I

II= Region II

III= Region III

Superscripts :

o= Outer solution

REFERENCES

1. D. E. White, L. J. Muffler and A. H. Trusdell, Vapor-dominated hydrothermal systems compared with hot-water systems, *Econ. Geol.* **66** (1), 75-97(1971).
2. C. H. Sondergeld and L. Turcotte, An experimental study of two phase convection in a porous medium with applications to geological problems, *J. Geophys. Res.* **82**, 2045-2053 (1977).
3. G. Schubert and J. M. Straus, Two-phase convection in a porous medium, *J. Geophys. Res.* **82**, 3411-3421 (1977).
4. N. E. Bixler and C. R. Carrigan, Enhanced heat transfer in partially-saturated hydrothermal systems, *Geophysical Res. Letters* **13**, 42-45 (1986).
5. M. Prats, *Thermal Recovery*, SPE Monograph, Vol. 7, Dallas, Texas (1982).
6. C. Doughty and K. Pruess, A semianalytical solution for heat-pipe effects near high-level nuclear waste packages buried in partially saturated geological media, *Int. J. Heat Mass Transfer* **31**, 79-90 (1988).
7. J. M. Buchlin, Transport Processes Associated with Nuclear Reactor Safety, Proceedings NATO/ASI on Transport in Porous Media (Y. Corapcioglu and J. Bear, eds.) Pullman, Wa. July 9-18 (1989).
8. E. E. Gomma and W. H. Somerton, The behavior of multifluid-saturated formations, Part II: Effect of vapor saturation-heat pipe concept and apparent, thermal conductivity, SPE Paper 4896-B, Proc. Soc. Petroleum Engineers, California Regional Meeting, San Francisco, April (1974).

9. Y. Ogniewicz and C. L. Tien, Porous heat pipe, in Heat Transfer, Thermal Control and Heat Pipes (Edited by W. B. Olstad), 70, Progress in Astronautics (Series Editor M. Summerfield) 329-345, AIAA, New York. Presented as paper 79-1093, AIAA 14th Thermophysics Conf., Orlando, Florida, June (1979).
10. V. Dhir and I. Catton, Dryout heat fluxes for inductively heated particulate beds, *J. Heat Transfer* 99, 250-256 (1977).
11. E. R. G. Eckert, R. J. Goldstein, A. I. Behbahani and R. Hain, Boiling in an unconstricted granular medium, *Int. J. Heat Mass Trans.*, 28, 1187-1196 (1985).
12. K. Cornwell, B. G. Nair and T. D. Patten, Observation of boiling in porous media, *Int. J. Heat Mass Transfer* 19, 236-238 (1976).
13. T. M. Shaw, Drying as an immiscible displacement process with fluid counterflow, *Physical Review Letters* 59, 1671 (1987)
14. F. G. Miller, Steady flow of two-phase single-component fluids through porous media, *Petroleum Trans., AIME* 192, 205 (1951).
15. J. C. Martin, R. E. Wegner and F. J. Kelsey, One-dimensional convective and conductive heat flow, Proceedings Second Workshop Geothermal Reservoir Engineering, Dec. 1-3, 1976.
16. G. Schubert and J. M. Straus, Steam-water counterflow in porous media, *J. Geophysical Res.* 84, 1621 1979.
17. H. H. Bau and K.E. Torrance, Boiling in low-permeability porous materials, *Int. J. Heat Mass Transfer* 25, 45-54 (1982).

18. K. S. Udell, Heat transfer in porous media heated from above with evaporation, condensation, and capillary effects, *J. Heat Trans.* 105, 485-492 (1983).

19. K. S. Udell, Heat transfer in porous media considering phase change and capillarity-the heat pipe effect, *Int. J. Heat Mass Transfer* 28, 485-495 (1985).

20. Y. C. Yortsos and M. Parlari, Phase change in porous media: Application to solution gas drive, paper SPE 19697 presented at the 64th Annual Technical Conference and Exhibition of SPE, San Antonio, TX, Oct. 8-11 (1989).

21. F. Kalaydjian, A macroscopic description of multi phase flow in porous media involving spacetime evolution of fluid/fluid interface, *Transport In Porous Media* 2, 537-552 (1987).

22. M. Parlari and Y. C. Yortsos, Percolation theory of steam-water relative permeability, paper SPE 16969 presented at the 62nd Annual Meeting of SPE, Dallas, TX, Sept. 27-30 (1987).

23. J. C. Melrose, Use of water vapor desorption data in the determination of capillary pressures, SPE 16286, *SPE Reservoir Engineering* 913-919 (1988).

24. C. M. Bender and S. A. Orszag, *Advanced Mathematical Methods for Scientists and Engineers*, McGraw Hill, New York (1978).

APPENDIX

The dimensionless constants c , e , f are obtained by a straightforward analysis.

We obtain

$$c = \frac{\beta R_p A_1 k_{rv}(S_{Lr})}{1 + k_{rv}(S_{Lr}) K R_m \frac{A_1}{\tau_1^2}} \quad (\text{I})$$

$$e = \frac{R_v + K R_p R_h \frac{A_1}{\tau_1^2}}{R_p A_1 J'(S_{Lr})} \quad (\text{II})$$

$$f = -\frac{nL}{\beta} J'(S_{Lr}) e^2 \quad (\text{III})$$

where A_1 and τ_1 pertain to conditions at ξ_1 . For typical parameter values [18] and $k = 1$ d, we obtain the estimates

$$c = 2.469 * 10^{-4} \quad , \quad e = 80.5169 \quad , \quad f = 3.0981 * 10^6$$

Table 1: Typical Parameter Values

$$S_{Lr} = 0.20$$

$$S_{Vr} = 0.05$$

$$T_o = 171.1 \text{ C}$$

$$P_o = 15 \text{ psi}$$

$$\sigma = 58.91 \text{ dynes/cm}$$

$$v_L = 18.76 \text{ cc/mole}$$

$$\rho_L = 0.9606 \text{ g/cm}^3$$

$$\rho_V = 0.0006 \text{ g/cm}^3$$

$$\mu_L = 2.824 \cdot 10^{-3} \text{ g/cm-sec}$$

$$\mu_V = 1.260 \cdot 10^{-4} \text{ g/cm-sec}$$

$$\lambda_I = 3.0 \text{ W/m-K}$$

$$\lambda_{III} = 1.2 \text{ W/m-K}$$

$$\lambda_{II} = \frac{\lambda_I - \lambda_{III}}{2} (1 - S_{Vr} - S_{Lr}) + \lambda_{III}$$

$$k_{rL} = \left(\frac{S - S_{Lr}}{1 - S_{Lr}} \right)^3$$

$$k_{rV} = \left(\frac{1 - S_{Vr} - S}{1 - S_{Vr}} \right)^3$$

$$P_c = 2.24 - 2.75S + 1.3S^2$$

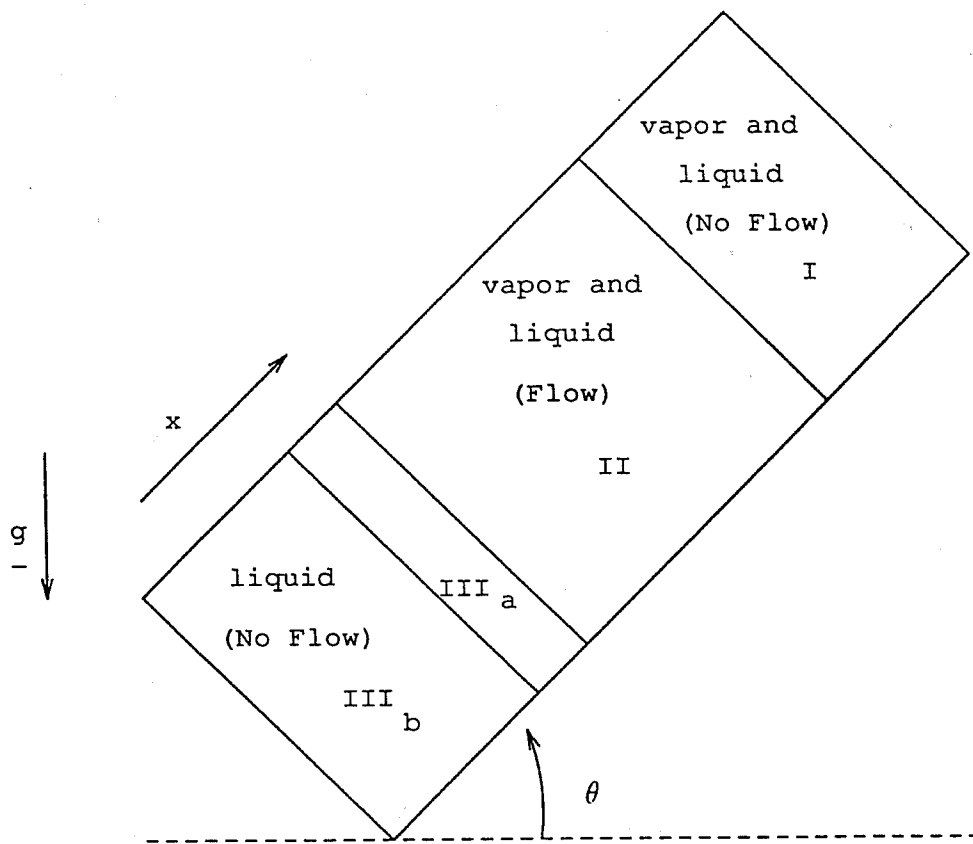


Figure 1. Countercurrent Flow Schematic.

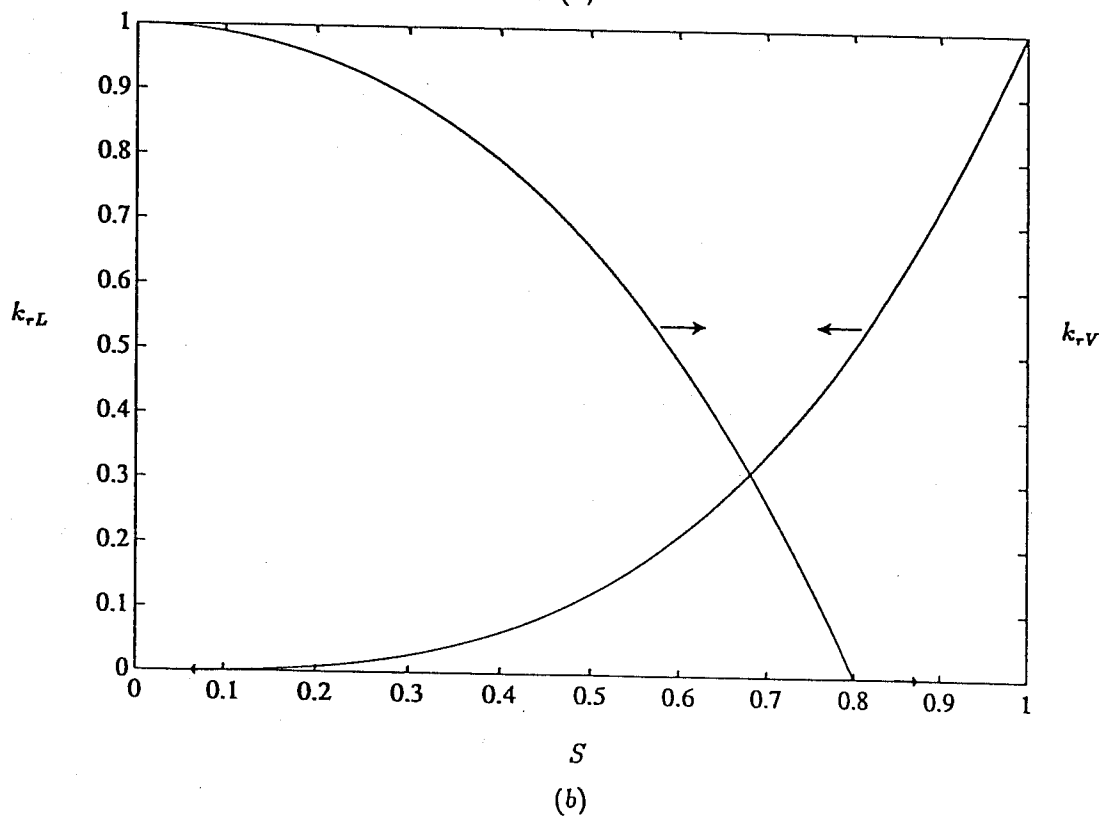
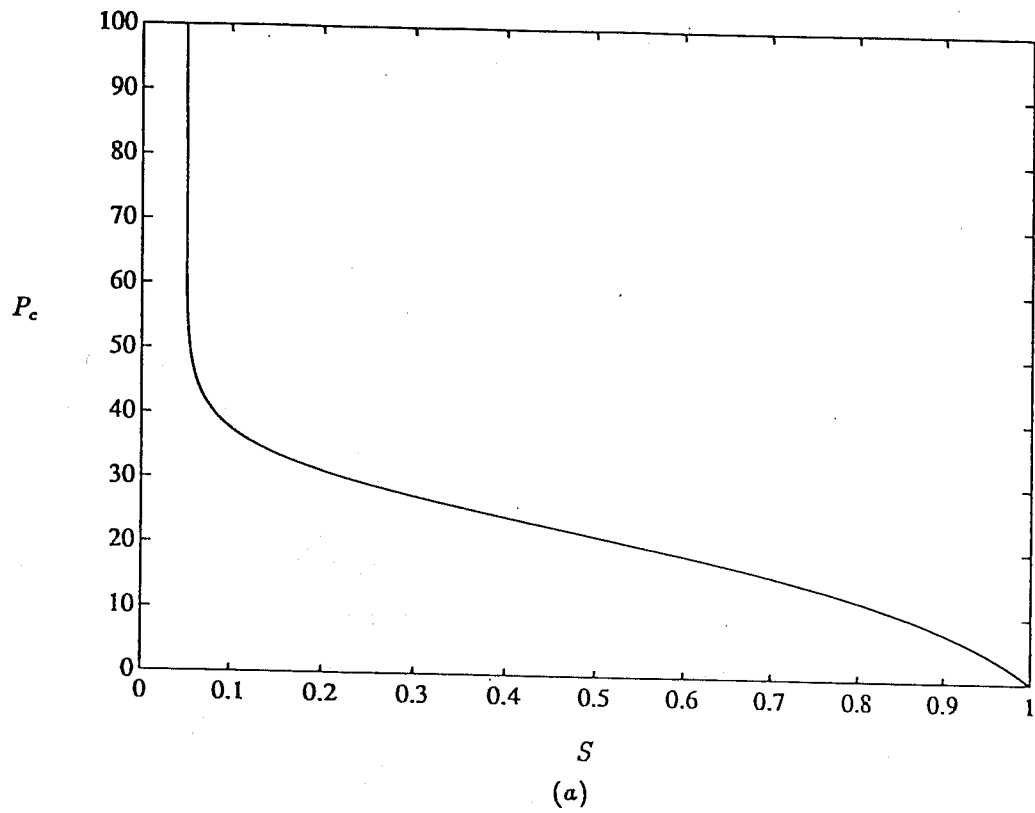


Figure 2. Schematics of Capillary Pressure (a) and Relative Permeability Curves (b).

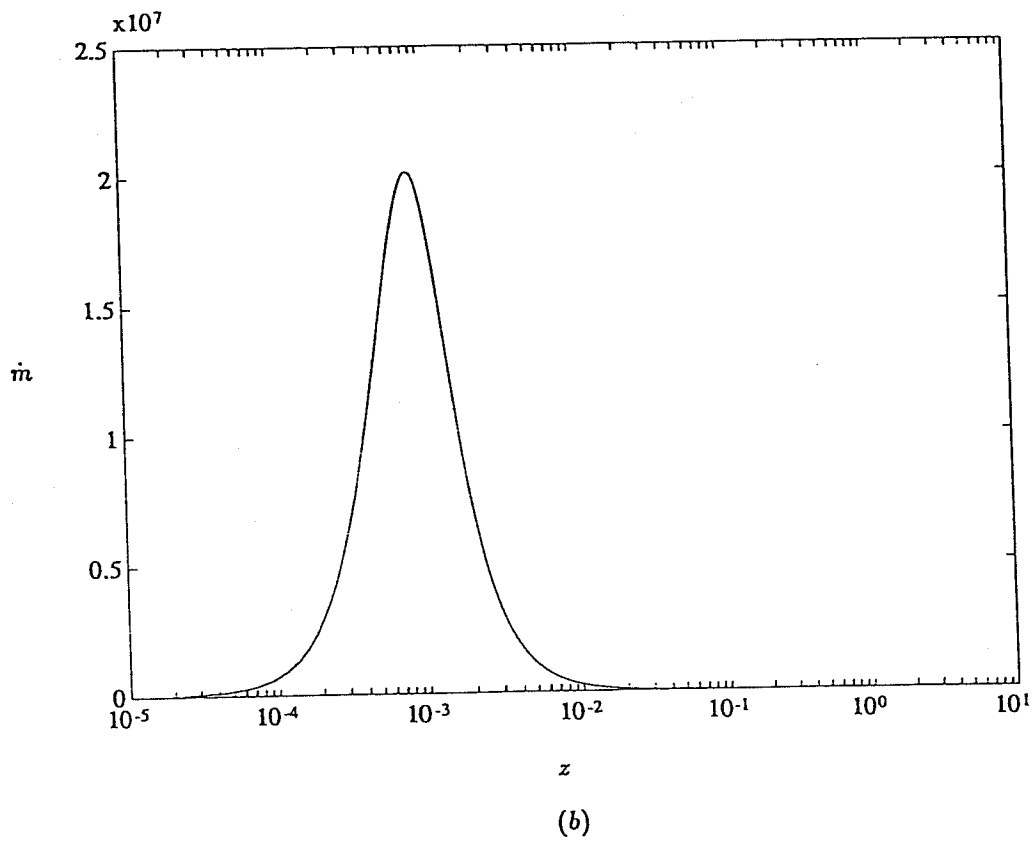
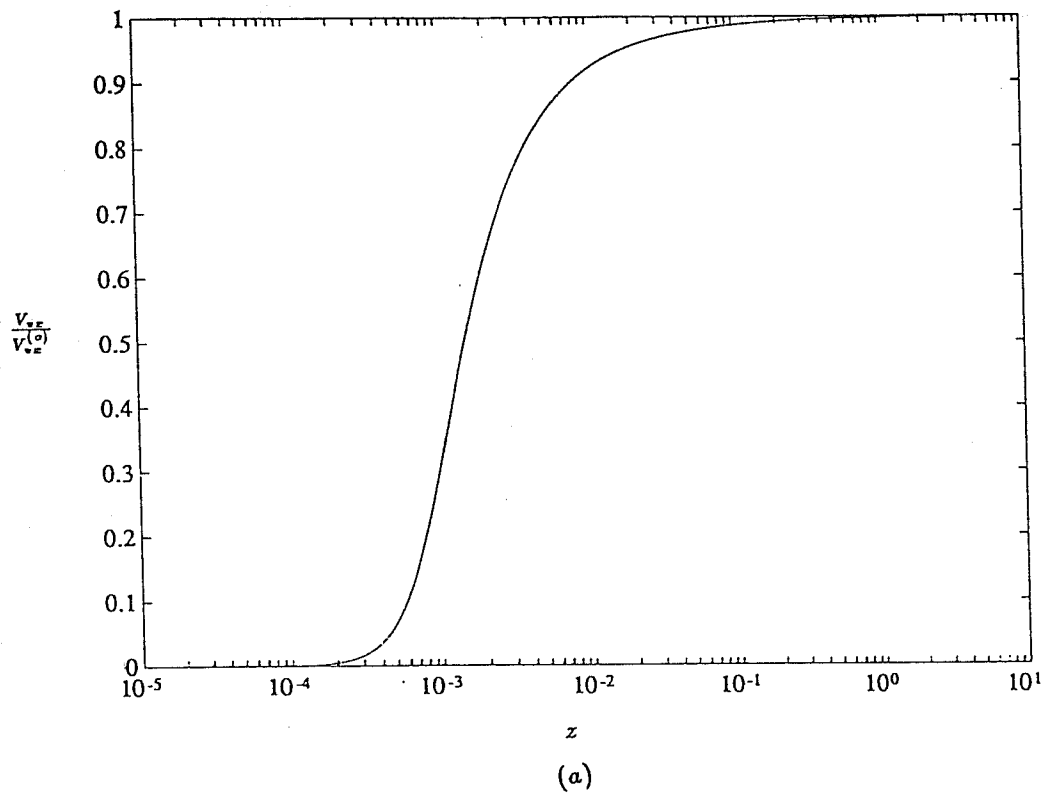


Figure 3. Boundary Layer Profiles: Normalized Vapor Flux (a) and Evaporation Rate (b).

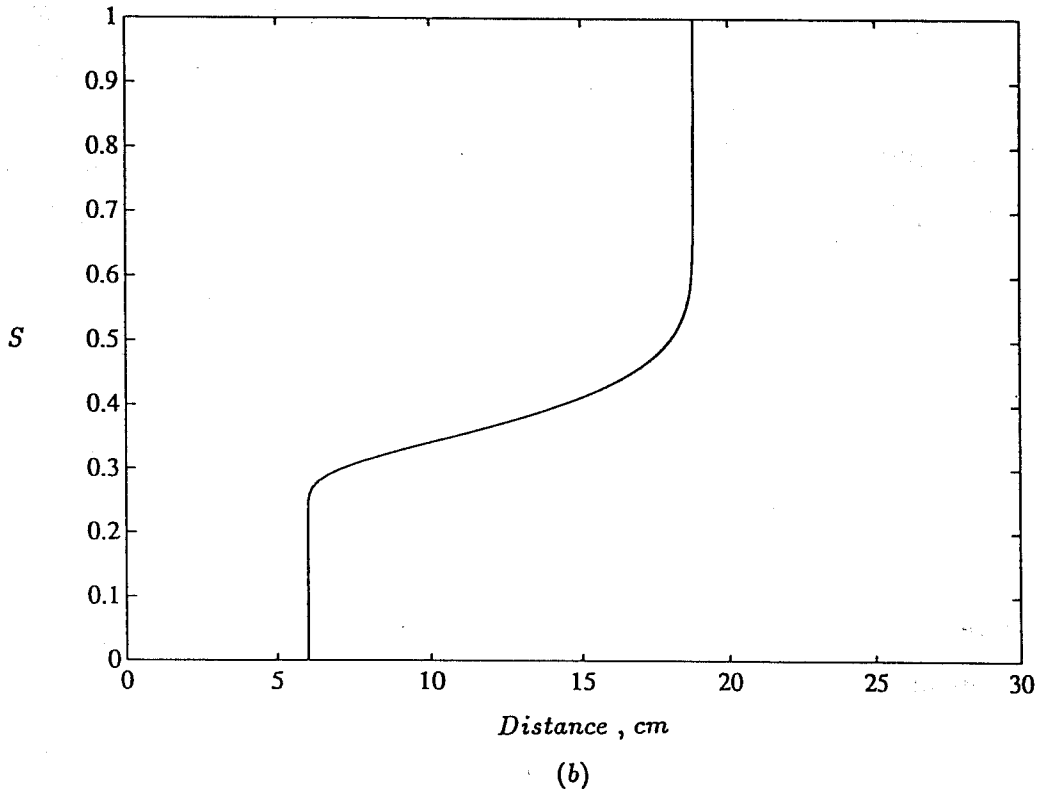
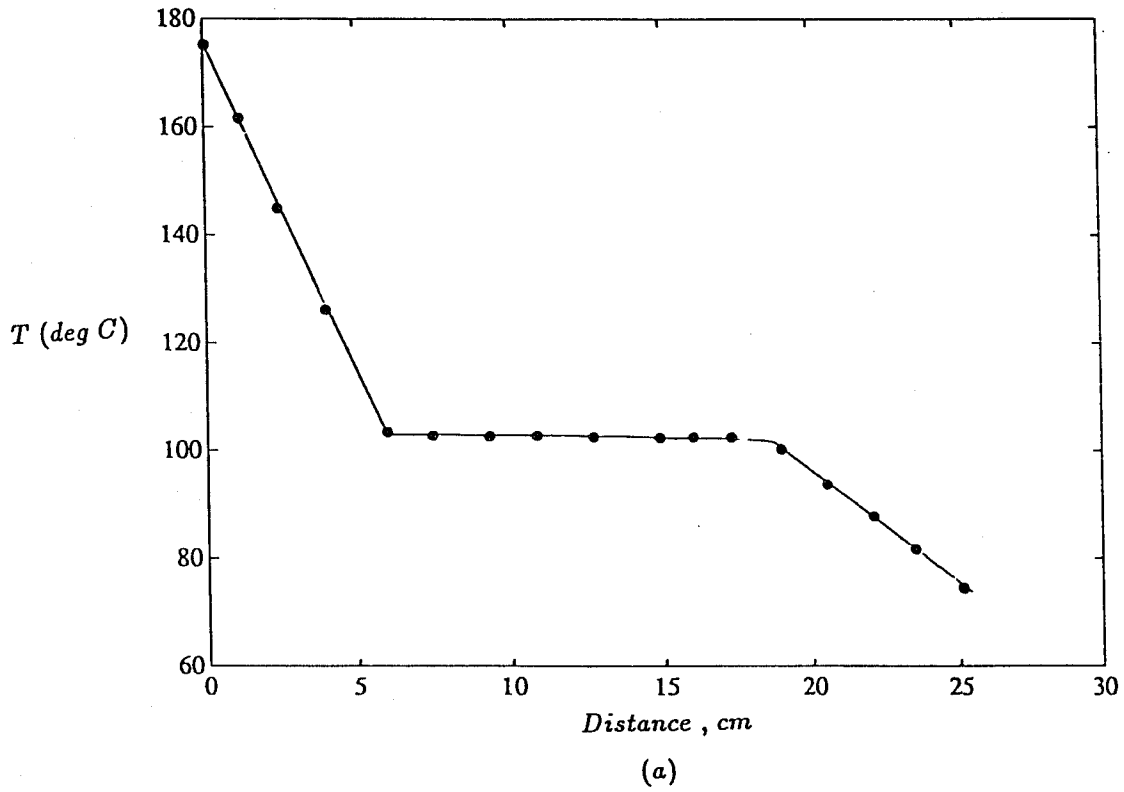


Figure 4. Profiles Corresponding to Ref. [18]: Temperature (a) and Liquid Saturation (b). Dots in (a) Correspond to Experimental Points [18].

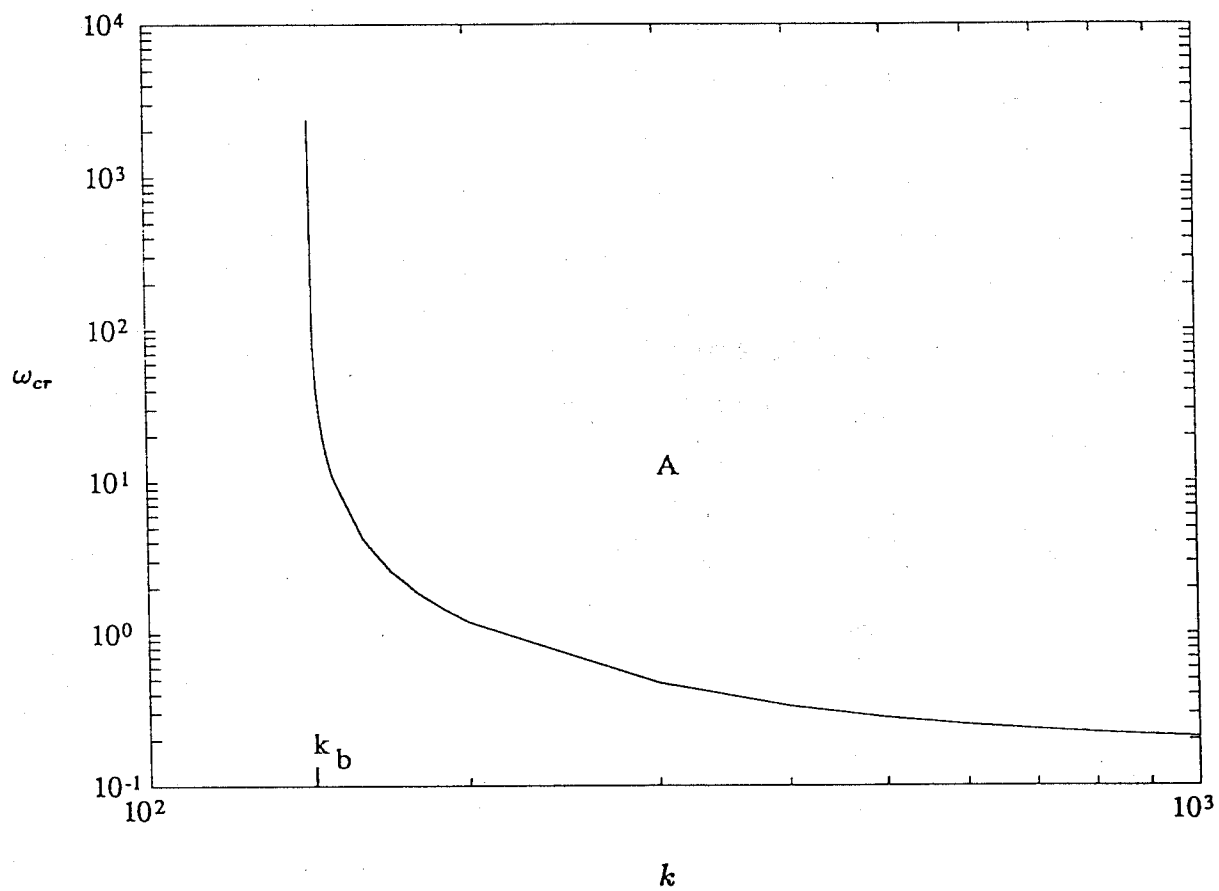


Figure 5. Critical Heat Flux as a Function of Permeability for Bottom Heating.

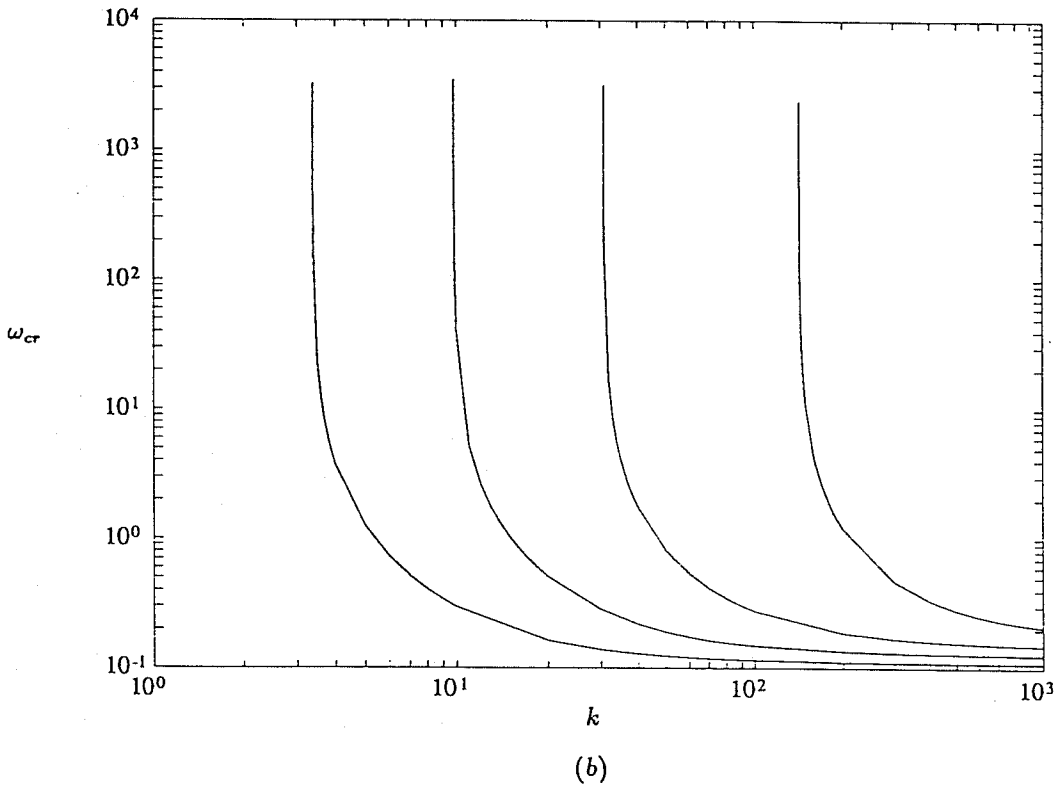
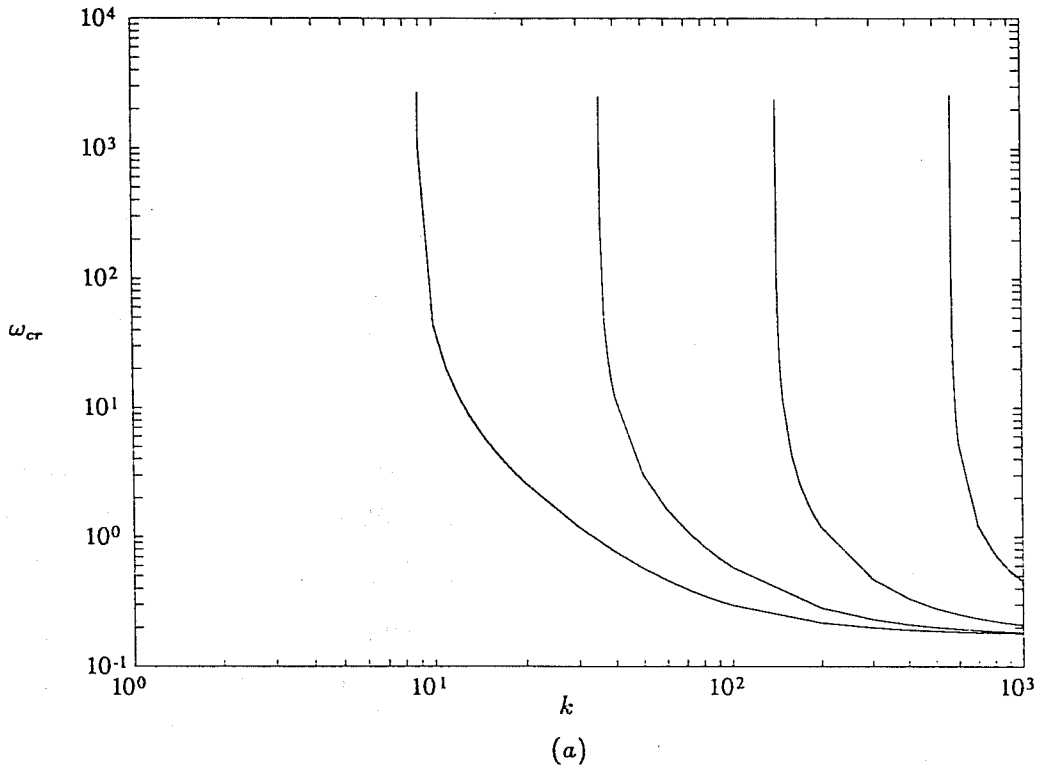


Figure 6. Effect of Surface Tension (a: $\sigma = 14.7275, 29.455, 58.91, 117.82$, from left to right) and Imposed Pressure (b: $P_o = 80, 50, 30, 15$, from left to right) on the Critical Heat Flux Curve.

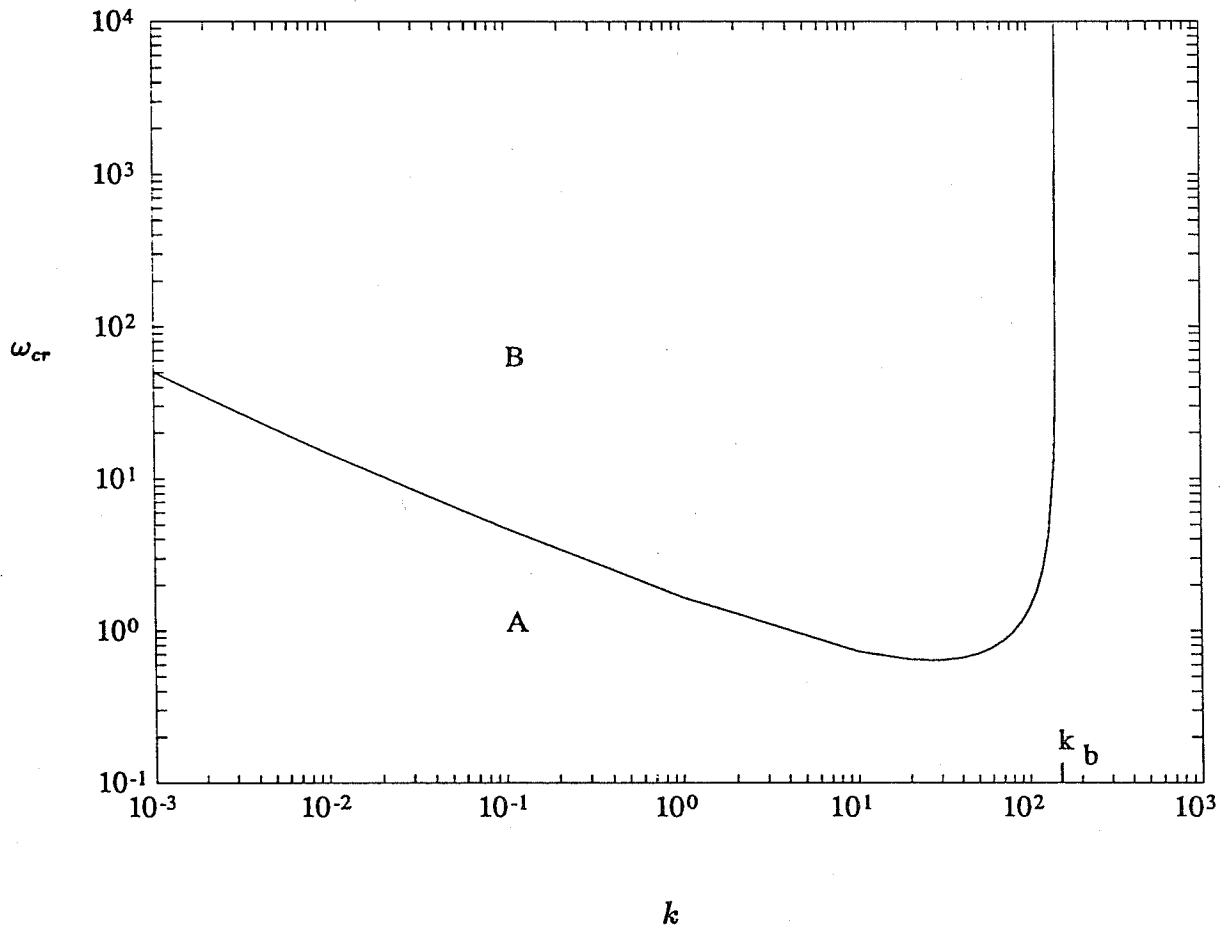


Figure 7. Critical Heat Flux as a Function of Permeability for Top Heating.

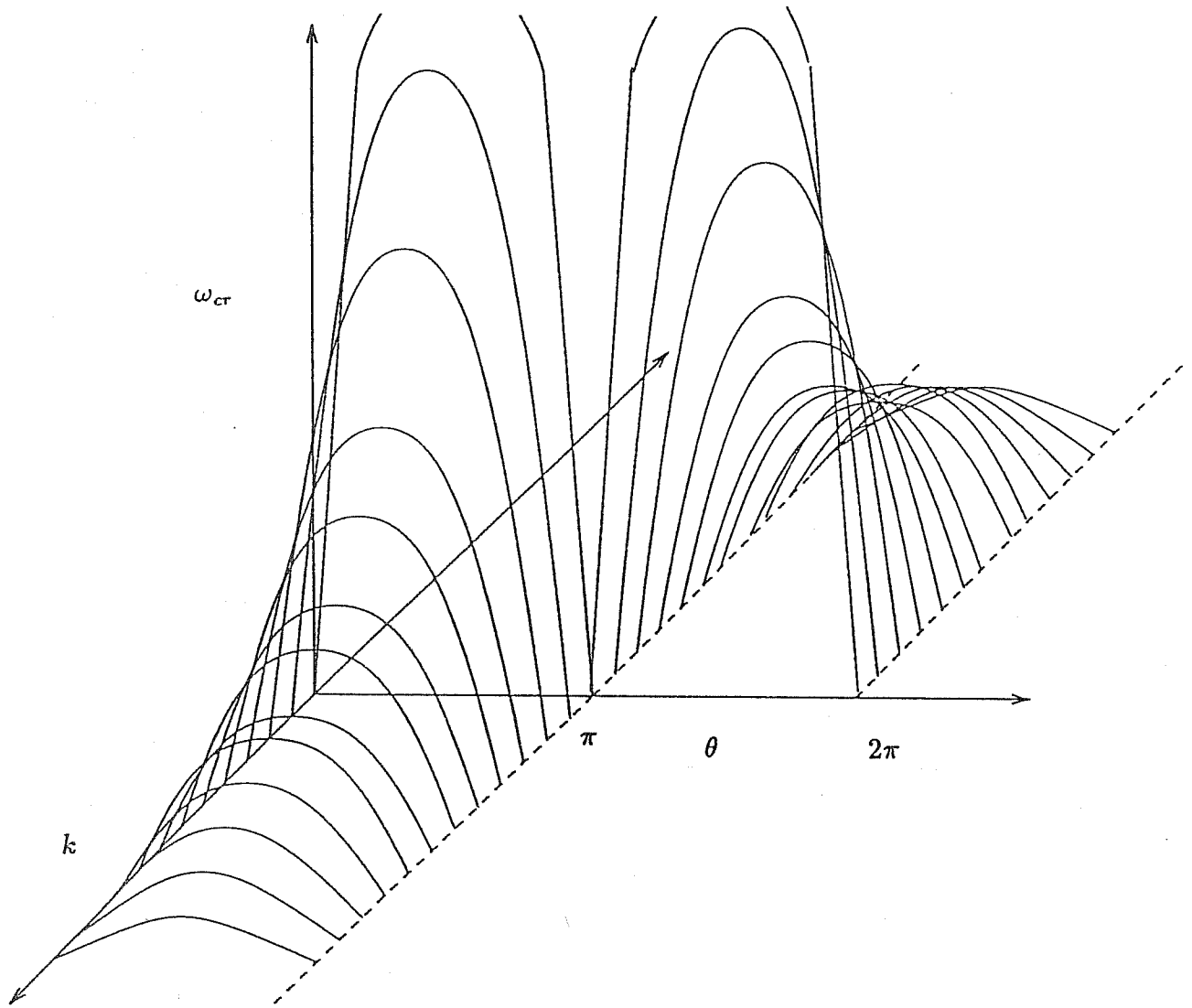
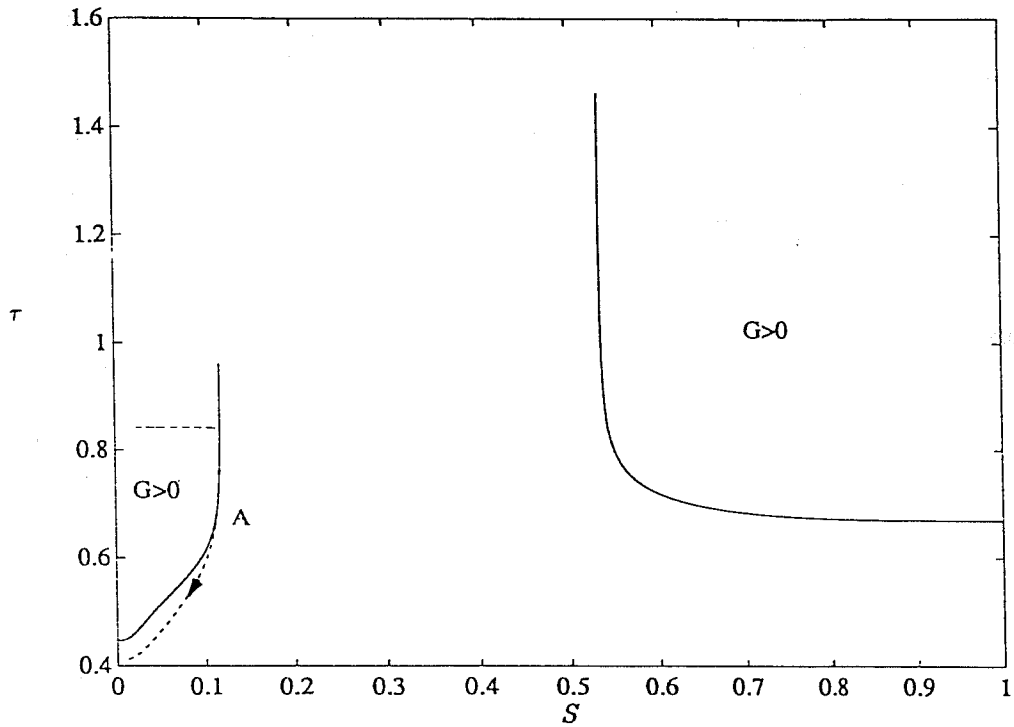
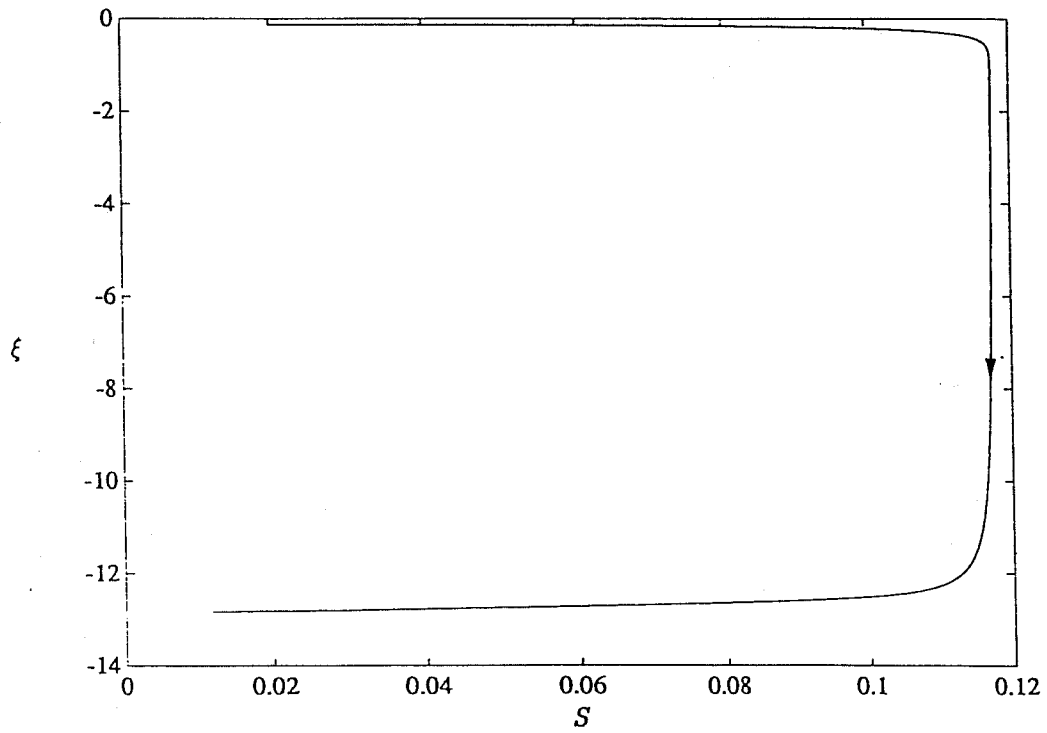


Figure 8. Composite Schematic of Critical Heat Flux Curve for Both Top and Bottom Heating.



(a)



(b)

Figure 9. Solution Trajectories for Bottom Heating and $\omega=0.1$: Temperature vs. Saturation (a) and Saturation vs. Distance (b). The Solid Curves in (a) Correspond to $G = 0$.

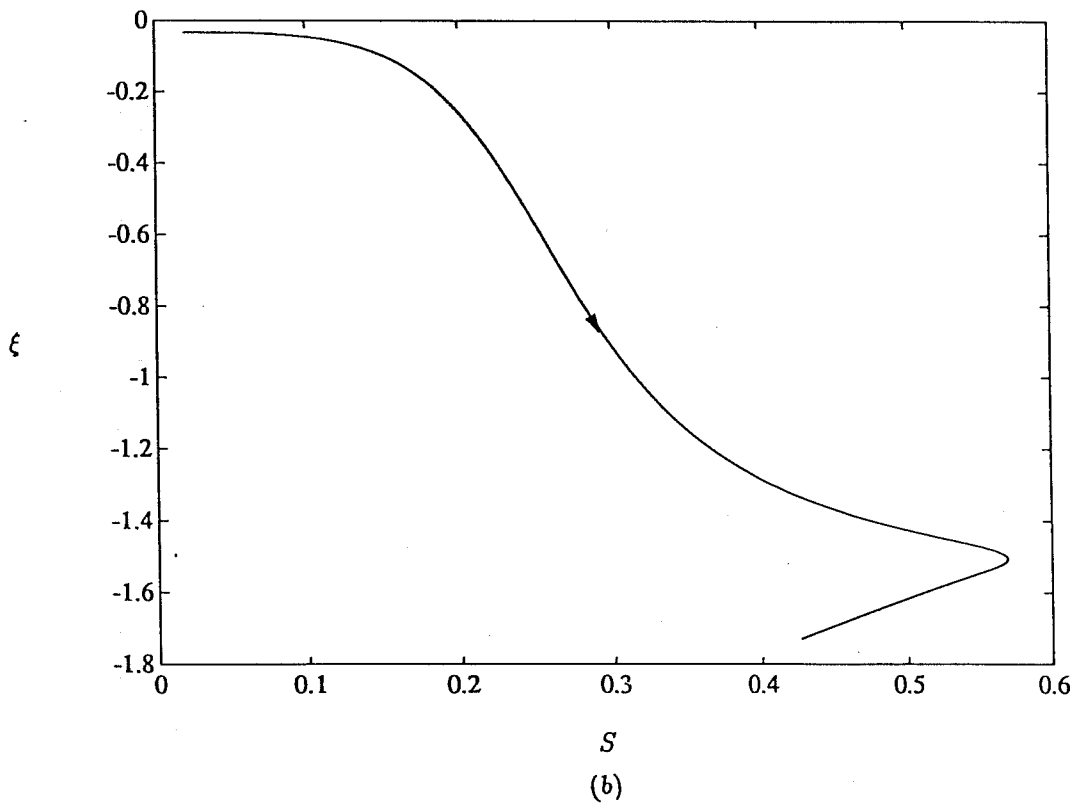
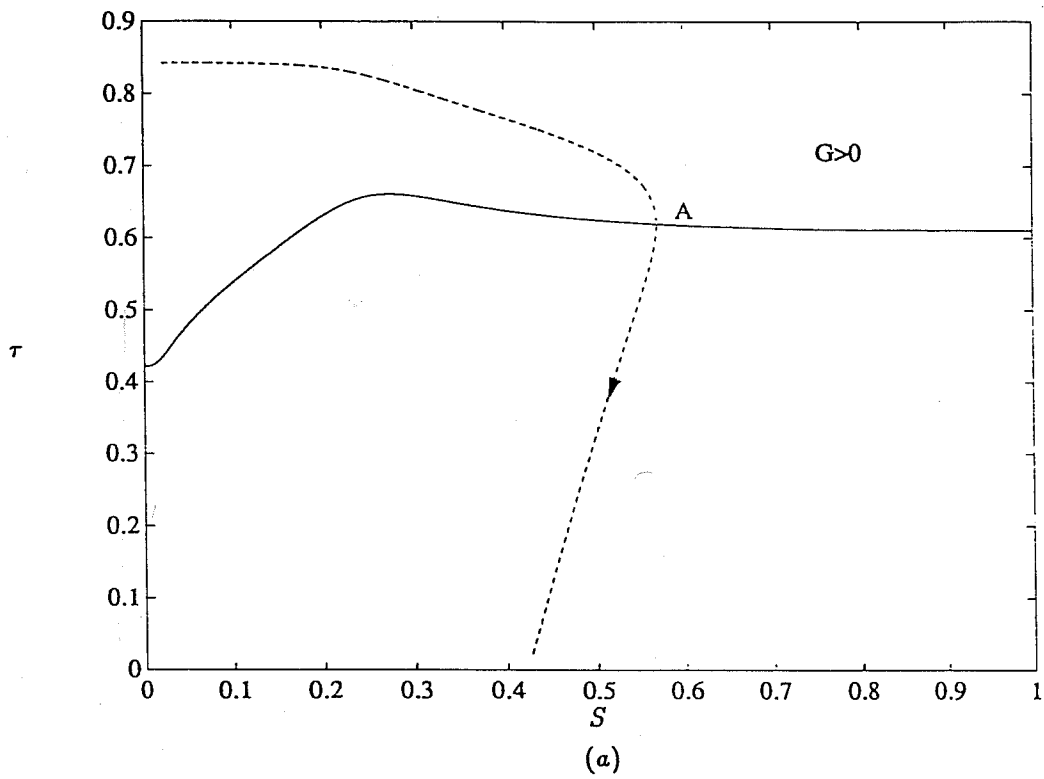
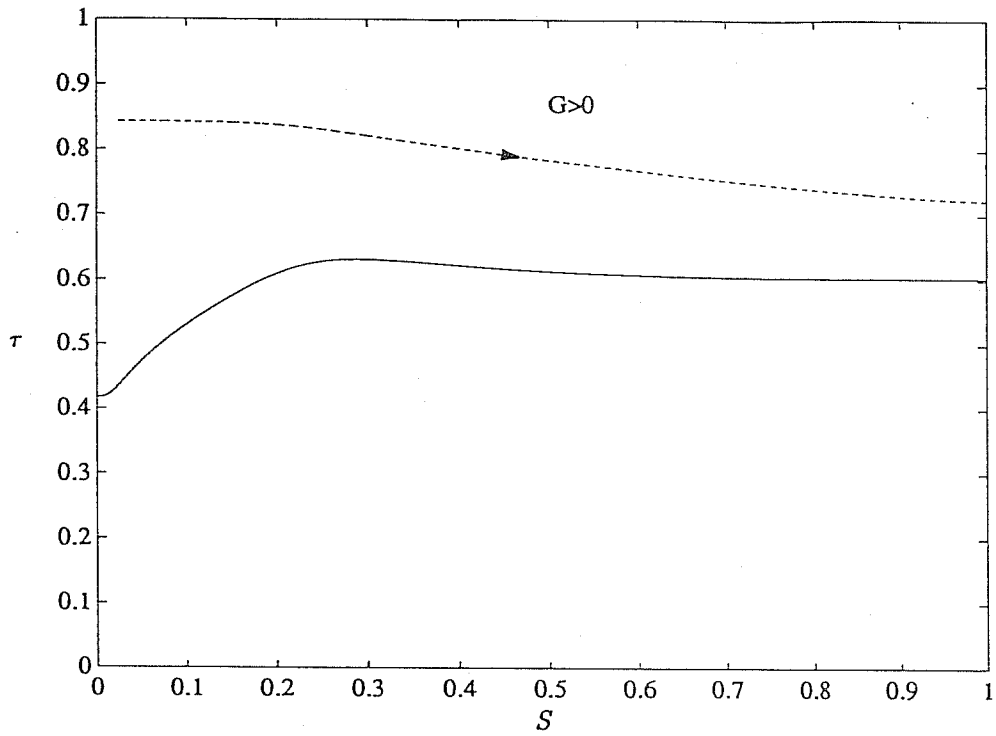
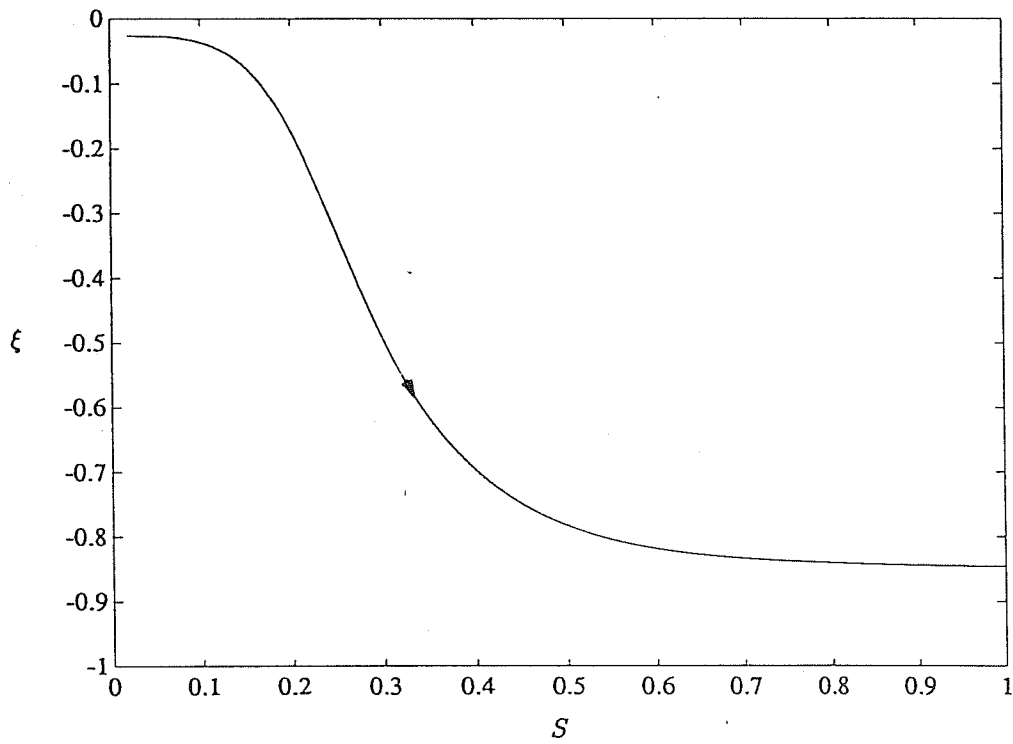


Figure 10. Solution Trajectories for Bottom Heating and $\omega=0.4$: Temperature vs. Saturation (a) and Saturation vs. Distance (b). The Solid Curves in (a) Correspond to $G = 0$.



(a)



(b)

Figure 11. Solution Trajectories for Bottom Heating and $\omega=0.5$: Temperature vs. Saturation (a) and Saturation vs. Distance (b). The Solid Curves in (a) Correspond to $G = 0$.

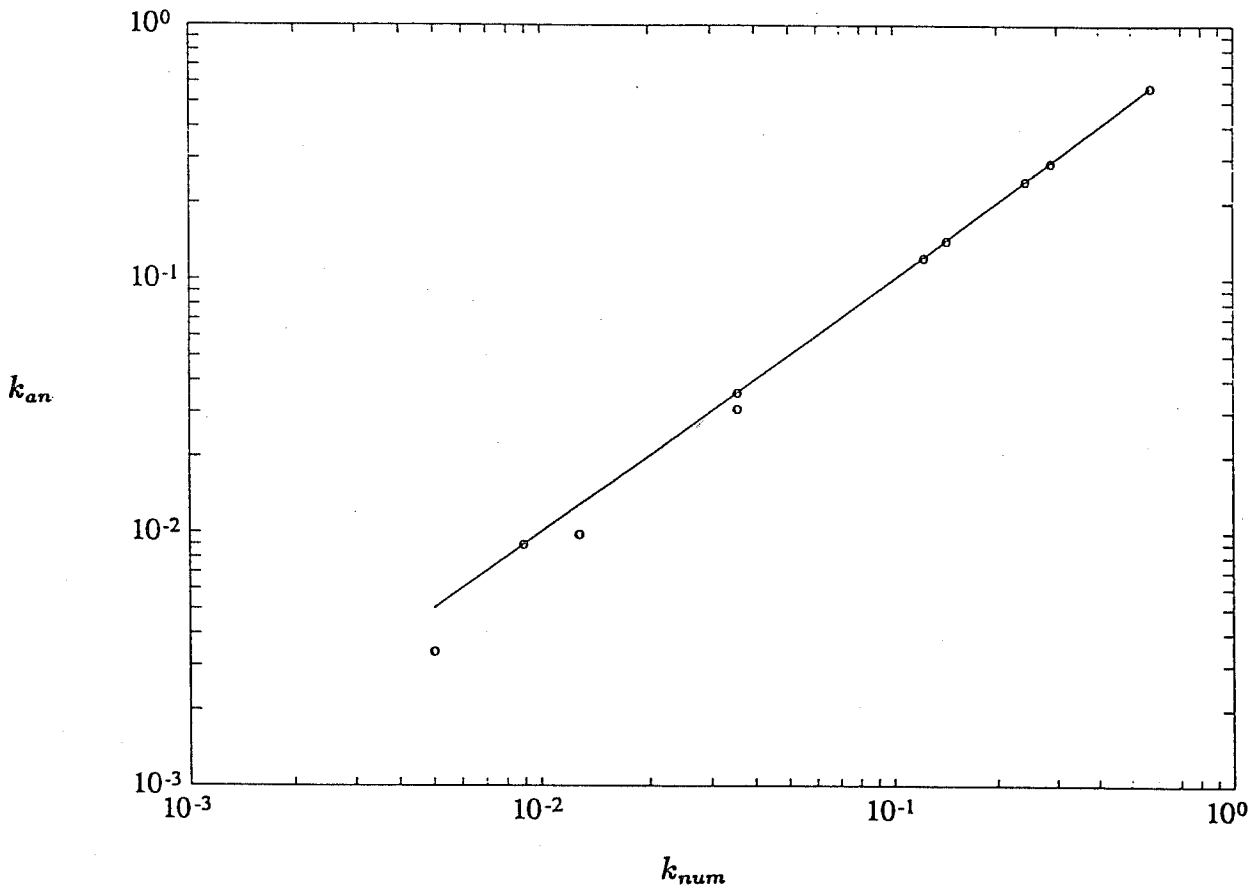


Figure 12. Numerical (Dots) and Analytical (Line) Predictions of Threshold Permeabilities for Variable Pressure, Interfacial Tension, Residual Saturations and Thermal Conductivities.

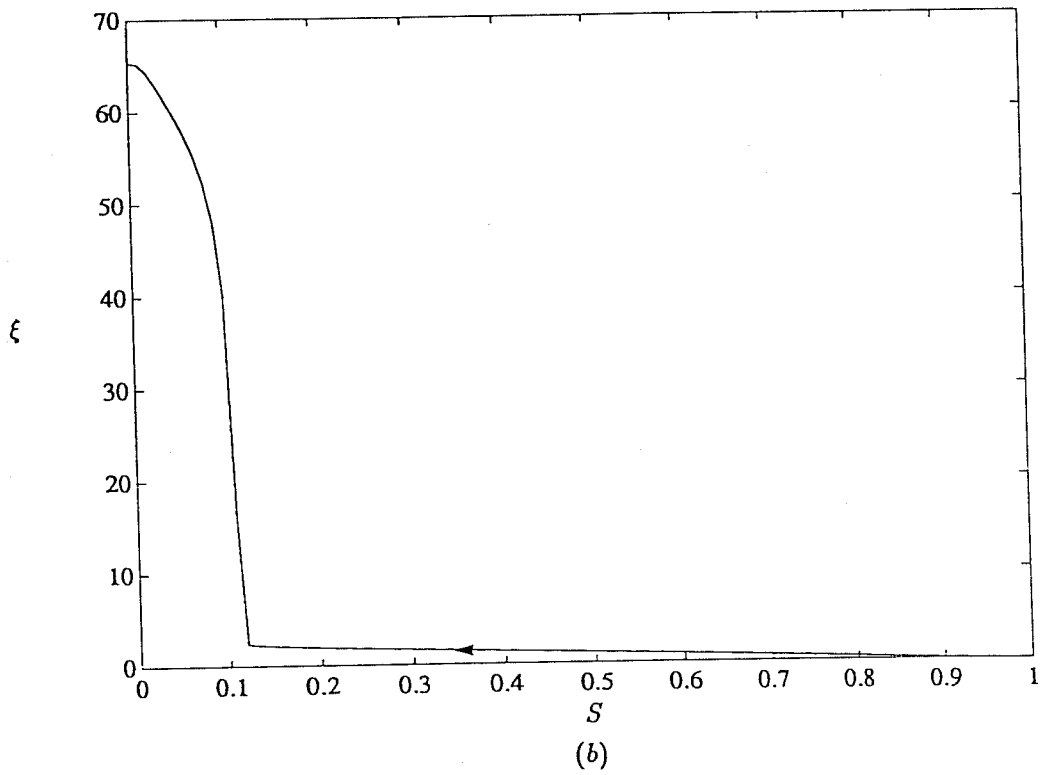
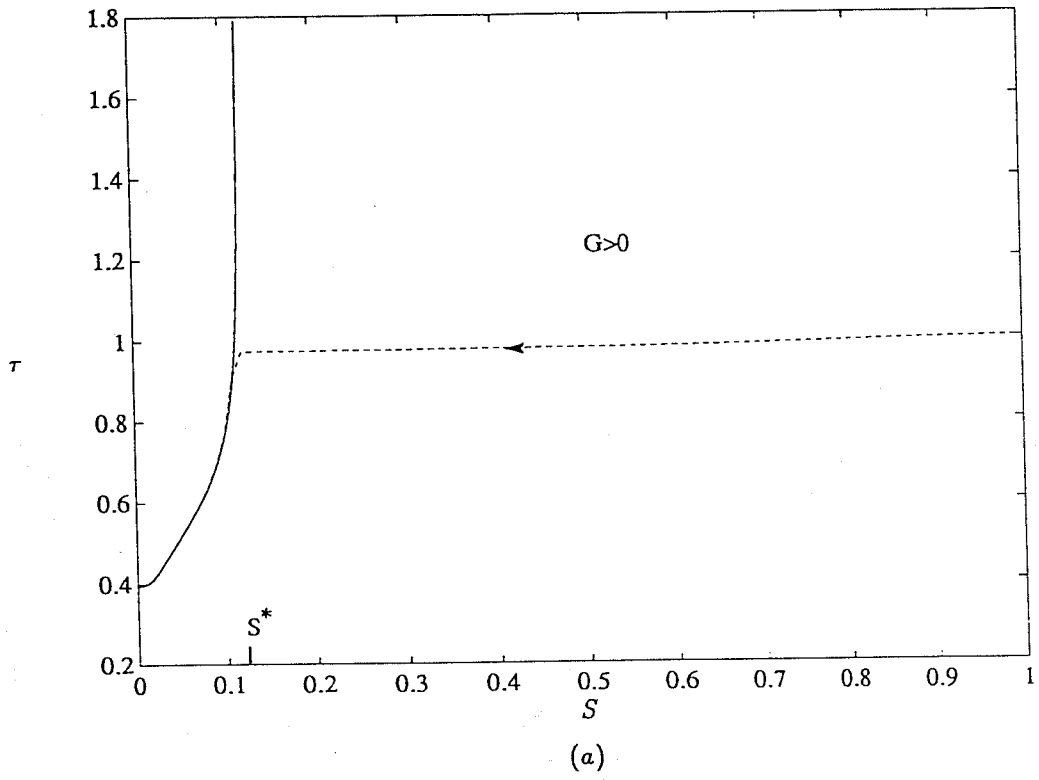


Figure 13. Solution Trajectories for the Geothermal Problem and $\epsilon = 0.0265275$: Temperature vs. Saturation (a) and Saturation vs. Distance (b). The Solid Curves in (a) Correspond to $G = 0$.

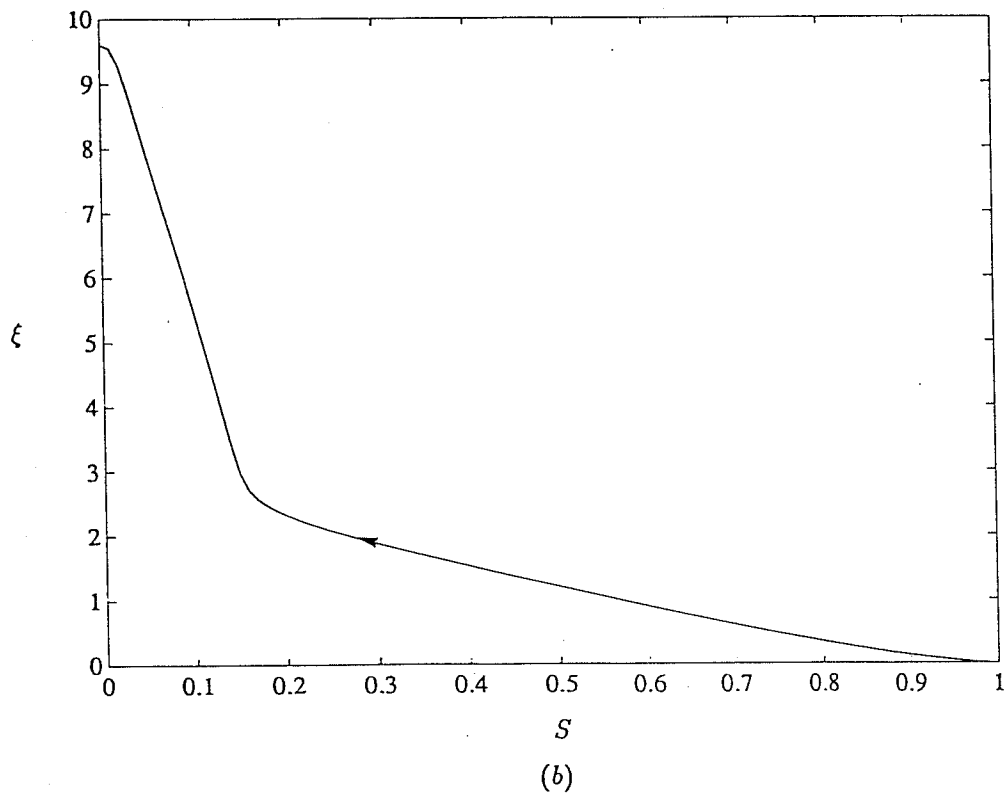
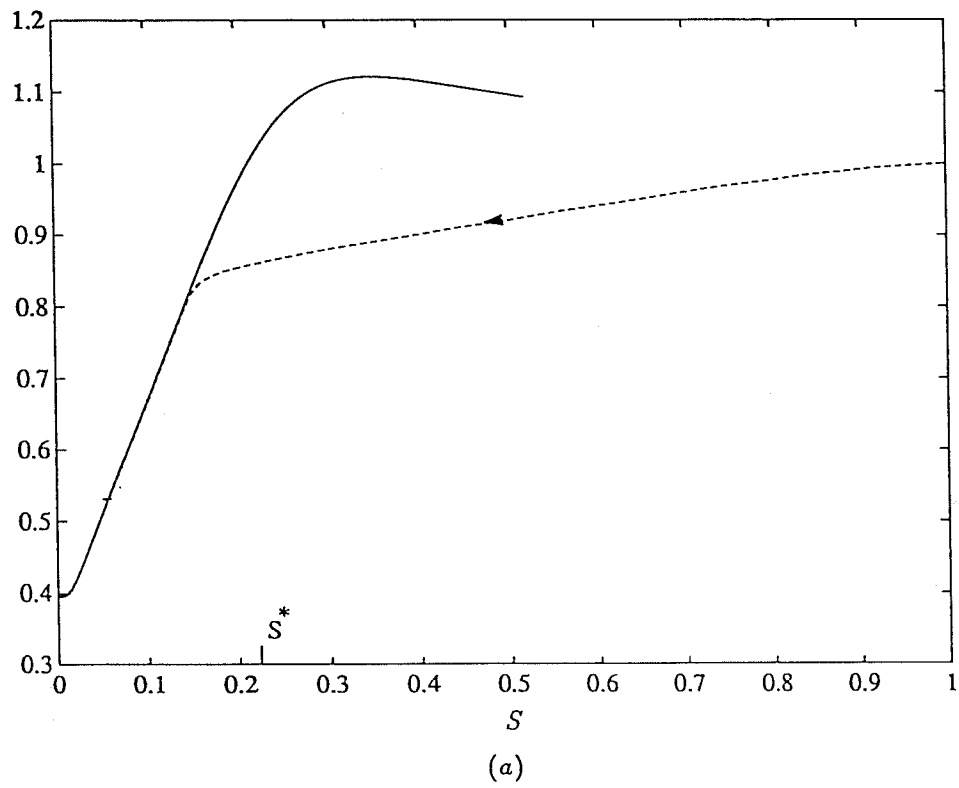


Figure 14. Solution Trajectories for the Geothermal Problem and $\epsilon = 0.0838876$: Temperature vs. Saturation (a) and Saturation vs. Distance (b). The Solid Curves in (a) Correspond to $G = 0$.

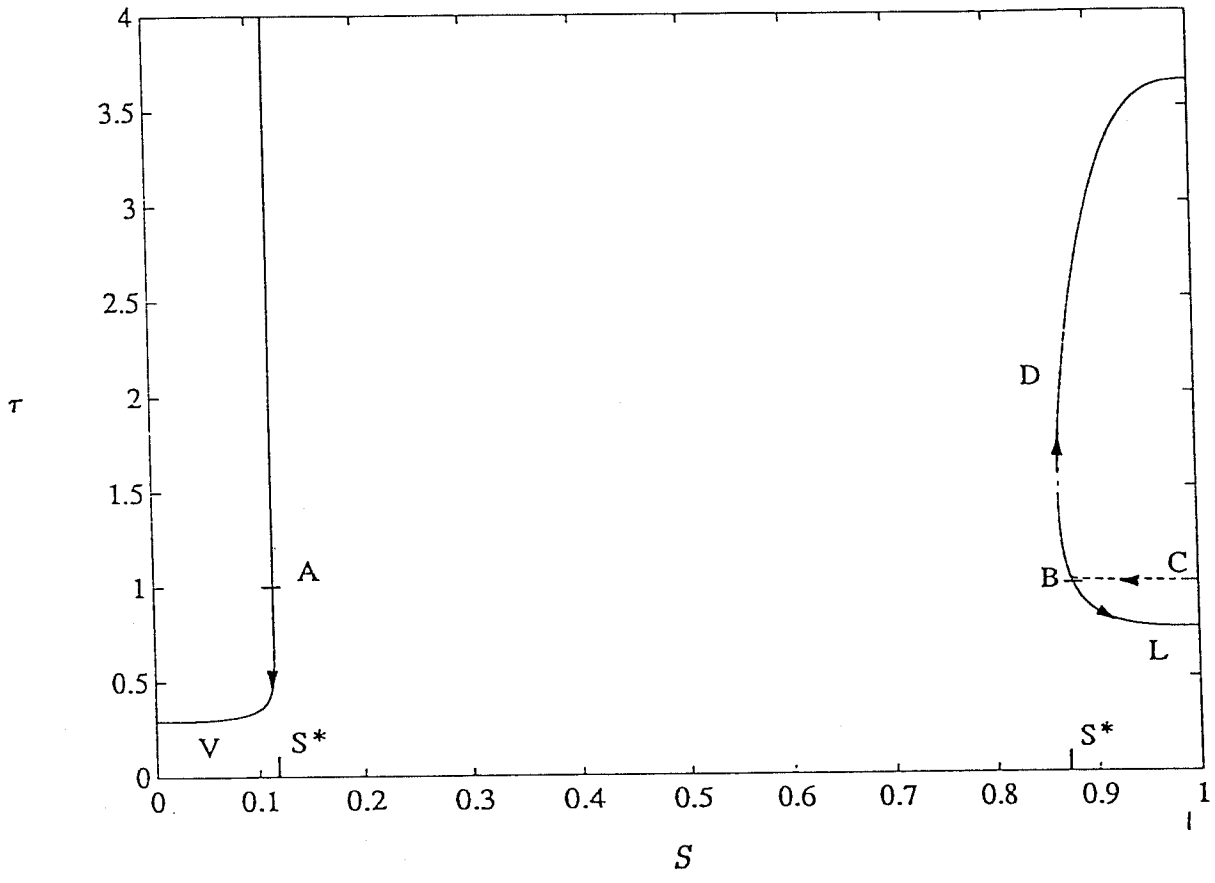


Figure 15. Solution Trajectories for the Geothermal Problem, with Heat Flux Exceeding the Limit (62): Temperature vs. Saturation. The Solid Curves Correspond to $G = 0$.

